



저작자표시-비영리-변경금지 2.0 대한민국

이용자는 아래의 조건을 따르는 경우에 한하여 자유롭게

- 이 저작물을 복제, 배포, 전송, 전시, 공연 및 방송할 수 있습니다.

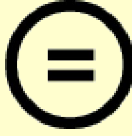
다음과 같은 조건을 따라야 합니다:



저작자표시. 귀하는 원저작자를 표시하여야 합니다.



비영리. 귀하는 이 저작물을 영리 목적으로 이용할 수 없습니다.



변경금지. 귀하는 이 저작물을 개작, 변형 또는 가공할 수 없습니다.

- 귀하는, 이 저작물의 재이용이나 배포의 경우, 이 저작물에 적용된 이용허락조건을 명확하게 나타내어야 합니다.
- 저작권자로부터 별도의 허가를 받으면 이러한 조건들은 적용되지 않습니다.

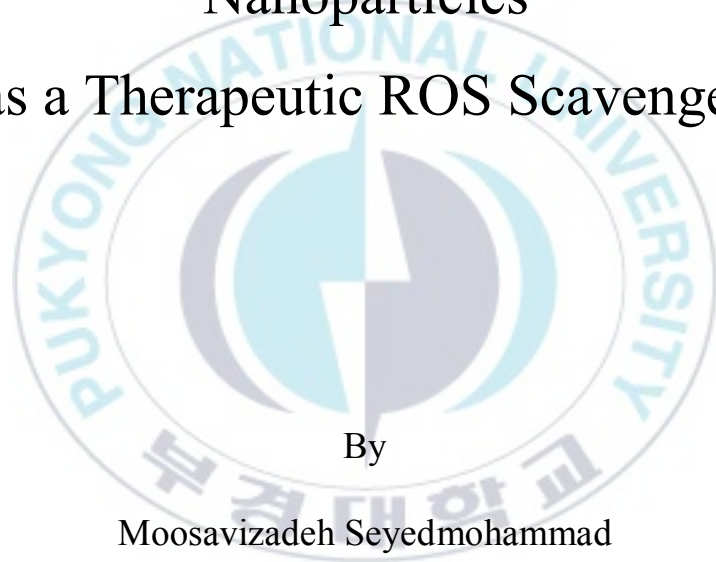
저작권법에 따른 이용자의 권리는 위의 내용에 의하여 영향을 받지 않습니다.

이것은 [이용허락규약\(Legal Code\)](#)을 이해하기 쉽게 요약한 것입니다.

[Disclaimer](#)

Thesis for the Degree of Master of Engineering

Bilirubin-Encapsulated Albumin  
Nanoparticles  
as a Therapeutic ROS Scavenger



By

Moosavizadeh Seyedmohammad

Department of Chemical Engineering

The Graduate School

Pukyong National University

August 2021

Bilirubin-Encapsulated Albumin  
Nanoparticles

as a Therapeutic ROS Scavenger.

(활성산소를 제거하는 빌리루빈 함유  
알부민 나노입자 제조와 치료적 응용)

Advisor: Prof. Sung In Lim

By

Moosavizadeh Seyedmohammad

A thesis submitted in partial fulfillment of the requirement  
for the degree of  
Master of Engineering  
in Department of Chemical Engineering, The Graduate School,  
Pukyong National University

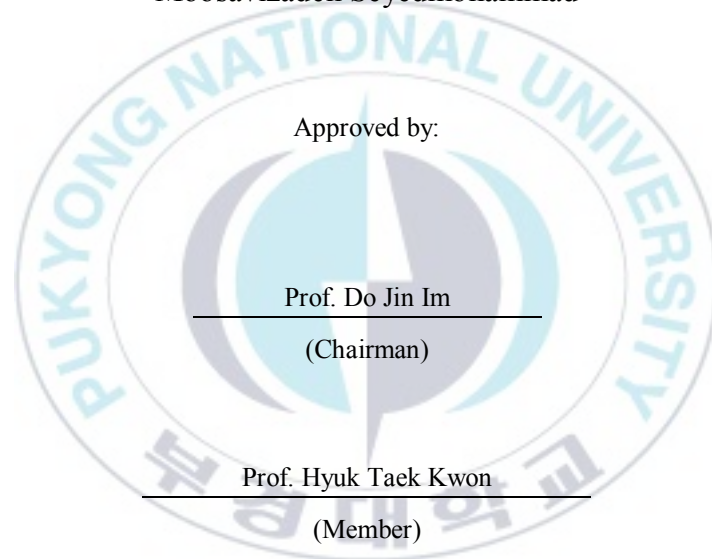
August, 2021

Bilirubin-Encapsulated Albumin Nanoparticles  
as a Therapeutic ROS Scavenger.

A dissertation

by

Moosavizadeh Seyedmohammad



Approved by:

Prof. Do Jin Im

---

(Chairman)

Prof. Hyuk Taek Kwon

---

(Member)

Prof. Sung In Lim

---

(Member)

August 27<sup>th</sup>, 2021

## ACKNOWLEDGEMENTS

This master's project could not have been performed without the support, instruction, and encouragement from my supervisor, colleagues, family, and friends. I want to take this opportunity to express my gratitude to all of them.

First of all, I would like to sincerely thank my supervisor, Professor Dr. Sung In Lim, for offering me an opportunity to perform this exciting topic in the Biomolecular Engineering and Biotherapeutics Laboratory, and his inspiring guidance and exceptional mentoring has provided throughout my time as his student.

I also would like to thank Professor Dr. Hyuk Taek Kwon for his patient support and valuable guidance and advice not only during my research but also in my life.

I would like to especially acknowledge Professor Dr. Dae Hee Lee and Gyu Hyeok Lee for their collaboration and valuable contribution to this project.

I would like to appreciate the board committee members, Professor Dr. Do Jin Lim and Professor Dr. Hyuk Taek Kwon.

I would like to dedicate this thesis to my wife and my parents for their love, endless support through the years, and encouraging and inspiring me to follow my dreams; I would not be the person I am today if you were not with me these years.

Finally, I want to extend my gratitude to all my friends for making my life more cheerful in Busan.



***Ever tried***  
***Ever failed***  
***No matter***  
***Try again***  
***Fail again***  
***Fail better***

-Samuel Beckett-

## TABLE OF CONTENTS

<b>ACKNOWLEDGEMENTS</b> .....	<b>i</b>
<b>TABLE OF CONTENTS</b> .....	<b>iii</b>
<b>LIST OF TABLES</b> .....	<b>vii</b>
<b>LIST OF FIGURES</b> .....	<b>viii</b>
<b>ABSTRACT</b> .....	<b>xi</b>
<b>FIGURE 1: GRAPHICAL ABSTRACT</b> .....	<b>xiii</b>
<b>CHAPTER 1: INTRODUCTION</b> .....	<b>1</b>
1.1. OXIDATIVE STRESS.....	2
1.1.1. OXIDATIVE STRESS AND FREE RADICALS.....	2
1.1.2. TARGETS OF OXIDATIVE STRESS.....	4
1.2. ALBUMIN.....	7
1.3. ALBUMIN NANOPARTICLES.....	11
1.4. BILIRUBIN.....	13
1.5. OBJECTIVES OF THIS STUDY.....	16

<b>CHAPTER 2: MATERIALS .....</b>	<b>17</b>
<b>CHAPTER 3: EXPERIMENTS .....</b>	<b>19</b>
3.1. NANOPARTICLES PREPARATION .....	20
3.1.1. NAKED-BSA NANOPARTICLES (BSA-NPS).....	21
3.1.2. BR-LOADED BSA NANOPARTICLES (BSA-BR-NPS).....	21
3.1.3. NANOPARTICLES PURIFICATION .....	23
3.2. NANOPARTICLES OPTIMIZATION .....	24
3.2.1. SOLVENT/NON-SOLVENT RATIO .....	24
3.3. NANOPARTICLES CHARACTERIZATION .....	24
3.3.1. YIELD%.....	24
3.3.2. SIZE.....	25
3.3.3. STABILITY.....	25
3.3.4. ZETA POTENTIAL.....	25
3.3.5. MORPHOLOGY .....	26
3.4. BILIRUBIN AND BILIVERDIN CALIBRATION.....	26
3.5. DRUG ENCAPSULATION.....	27
3.5.1. ABSORBANCE.....	27
3.5.2. ENCAPSULATION EFFICIENCY and DRUG LOADING .....	28

3.6. RELEASE ASSAY .....	28
3.7. FREE-RADICAL SCAVENGING.....	30
3.7.1. DPPH FREE-RADICAL SCAVENGING ACTIVITY .....	30
3.7.2. ABTS FREE-RADICAL SCAVENGING ACTIVITY .....	31
3.8. CELL ASSAY .....	31
3.8.1. MTT ASSAY.....	31
<b>CHAPTER 4: RESULTS.....</b>	<b>34</b>
4.1. NANOPARTICLES PREPARATION AND OPTIMIZATION.....	35
4.2. NANOPARTICLES CHARACTERIZATION.....	35
4.3. STANDARD CALIBRATION .....	46
4.4. DRUG ENCAPSULATION.....	47
4.5. RELEASE ASSAY .....	50
4.6. FREE-RADICAL SCAVENGING.....	53
4.6.1. DPPH FREE-RADICAL SCAVENGING ACTIVITY .....	53
4.6.2. ABTS FREE-RADICAL SCAVENGING ACTIVITY .....	54
4.7. CELL ASSAY .....	56
4.7.1. MTT ASSAY.....	56
<b>CHAPTER 5: DISCUSSION AND CONCLUSION .....</b>	<b>67</b>

요약.....75

CHAPTER 6: REFERENCES .....77



## LIST OF TABLES

Table 1.1. Serum albumin binding sites

Table 4.1. NPS Optimization, Solvent : Non-Solvent ratio

Table 4.2. NPs characterization, Yield %

Table 4.3. NPs characterization, Dynamic Light Scattering

Table 4.4. NPs characterization, E.E %

Table 4.5. NPs characterization, D.L %

Table 4.6. BR derivatives comparison



## LIST OF FIGURES

Figure 1.1. GRAPHICAL ABSTRACT

Figure 1.2. Oxidative Stress and ROS mechanism

Figure 1.3. Blood components and plasma proteins

Figure 1.4. Serum albumin 3D structure (Copy right: Albumedix Ltd.)

Figure 1.5. Cys34 binding site and antioxidant activity

Figure 1.6. Albumin nanoparticles advantages

Figure 1.7. Desolvation technique

Figure 1.8. Bilirubin metabolism

Figure 3.1. Nanoparticles Preparation Process

Figure 3.2. PH Adjustment in BSA-BR-NPS preparation Process

Figure 3.3. BR release assay from BSA-BR-NPs

Figure 4.1. BSA-NPs characterization, Size

Figure 4.2. BSA-NPs characterization, Zeta Potential

Figure 4.3. BSA-NPs characterization, Size Stability

Figure 4.4. BSA-BR-NPs characterization, Size

Figure 4.5. BSA-BR-NPs characterization, Zeta Potential

Figure 4.6. BSA-BR-NPs characterization, Stability

Figure 4.7. BSA- NPs characterization, TEM

Figure 4.8. BSA- BR-NPs characterization, TEM

Figure 4.9. BSA-NPs characterization, SEM

Figure 4.10. BSA-BR-NPs characterization, SEM

Figure 4.11. BR standard curve

Figure 4.12. BV standard curve

Figure 4.13. BSA-BR-NPs, Drug encapsulation, a wave scan

Figure 4.14. BR release profile from BSA-BR-NPs in Normal Condition

Figure 4.15. BR release profile from BSA-BR-NPs in Inflammation Condition

Figure 4.16. BR release profile from BSA-BR-NPs, Comparison

Figure 4.17. DPPH radical scavenging

Figure 4.18. ABTS radical scavenging

Figure 4.19. MTT-assay on CCD18-co cell line

Figure 4.20. MTT-assay on BEAS-2B cell line

Figure 4.21. MTT-assay on NHA cell line

Figure 4.22. MTT-assay on DLD-1 cell line

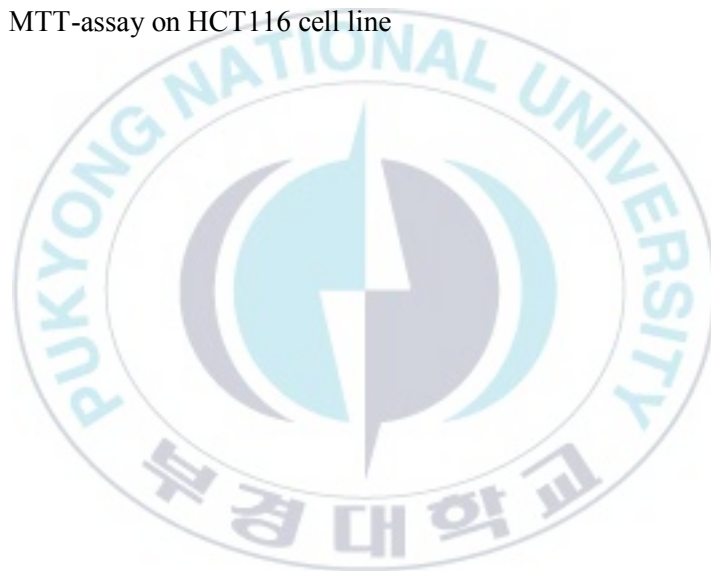
Figure 4.23. MTT-assay on LN229cell line

Figure 4.24. MTT-assay on SKOV-3 cell line

Figure 4.25. MTT-assay on CAOV-3cell line

Figure 4.26. MTT-assay on SW480 cell line

Figure 4.27. MTT-assay on HCT116 cell line



Bilirubin-Encapsulated Albumin Nanoparticles as a Therapeutic ROS scavenger.

Moosavizadeh Seyedmohammad

Department of Chemical Engineering, The Graduate School,

Pukyong National University

## ABSTRACT

Bilirubin (BR) is a bile pigment and the end-product of heme catabolism which occurs abundantly in the blood plasma. Bilirubin is an endogenous antioxidant capable of scavenging different reactive oxygen species (ROS) and free radicals, thereby playing a role in protecting the cells and tissues from oxidative damage. Indeed, numerous experimental studies proved the potential of bilirubin for antioxidant, anti-inflammatory, and anticancer activities. However, its low water-solubility, toxicity on normal cells, rapid clearance, and high sensitivity to oxygen restrict further clinical developments, requiring an appropriate drug carrier capable of stably encapsulating and delivering a defined dosage to the site of action.

Albumin is the most abundant protein in blood with a long circulatory half-life due to its size and FcRn binding property. Albumin has the capability to bind nutrients, metabolites, metals, and drugs, lending itself to a promising carrier that can affect the pharmacokinetics of the payload. Moreover, albumin is localized explicitly to tumors or inflamed tissues in either an active or a passive manner. Recently, serum albumin nanoparticles, i.e., BSA-NPs, have been used for delivering various types of therapeutic agents encapsulated inside or modified on the surface.

This study explored how to synthesize and characterize albumin nanoparticles encapsulating hydrophobic bilirubin by the desolvation method. In addition, we measured its ROS scavenging, biocompatibility, and toxicity on cancerous cells.

Using this method, albumin nanoparticles encapsulating bilirubin (BSA-BR-NPS) with a stable size around 164 nm and a spherical morphology obtained with a high yield of around 70%. The entrapment efficiency (EE) was around 66%, and the drug loading (DL) was around 11%. The BSA-BR-NPs could scavenge more than 90% of the free radicals in radical scavenging measurement. The in vitro cellular assay of nanoparticles on different normal cells showed low toxicity on normal cells, which approved its biocompatibility. On the other hand, the BSA-BR-NPs had significant toxicity on cancerous cells. These results demonstrated that BSA-BR-NPS improved and optimized therapeutic efficiency of BR by addressing its limitations.

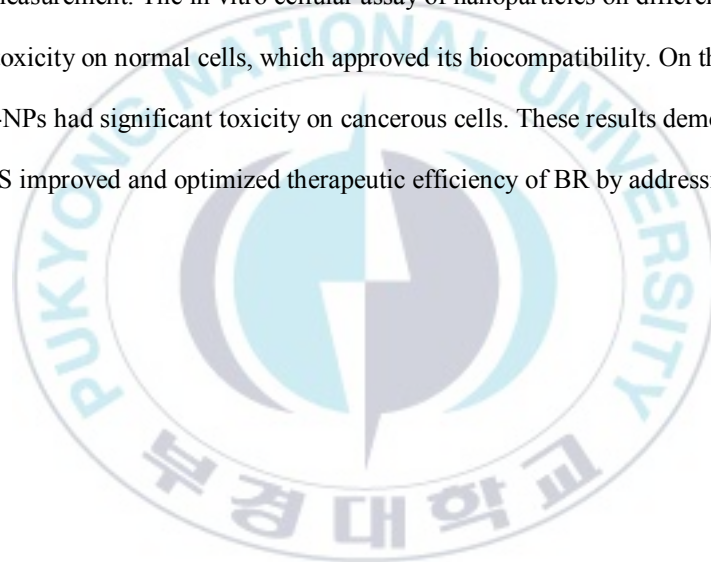
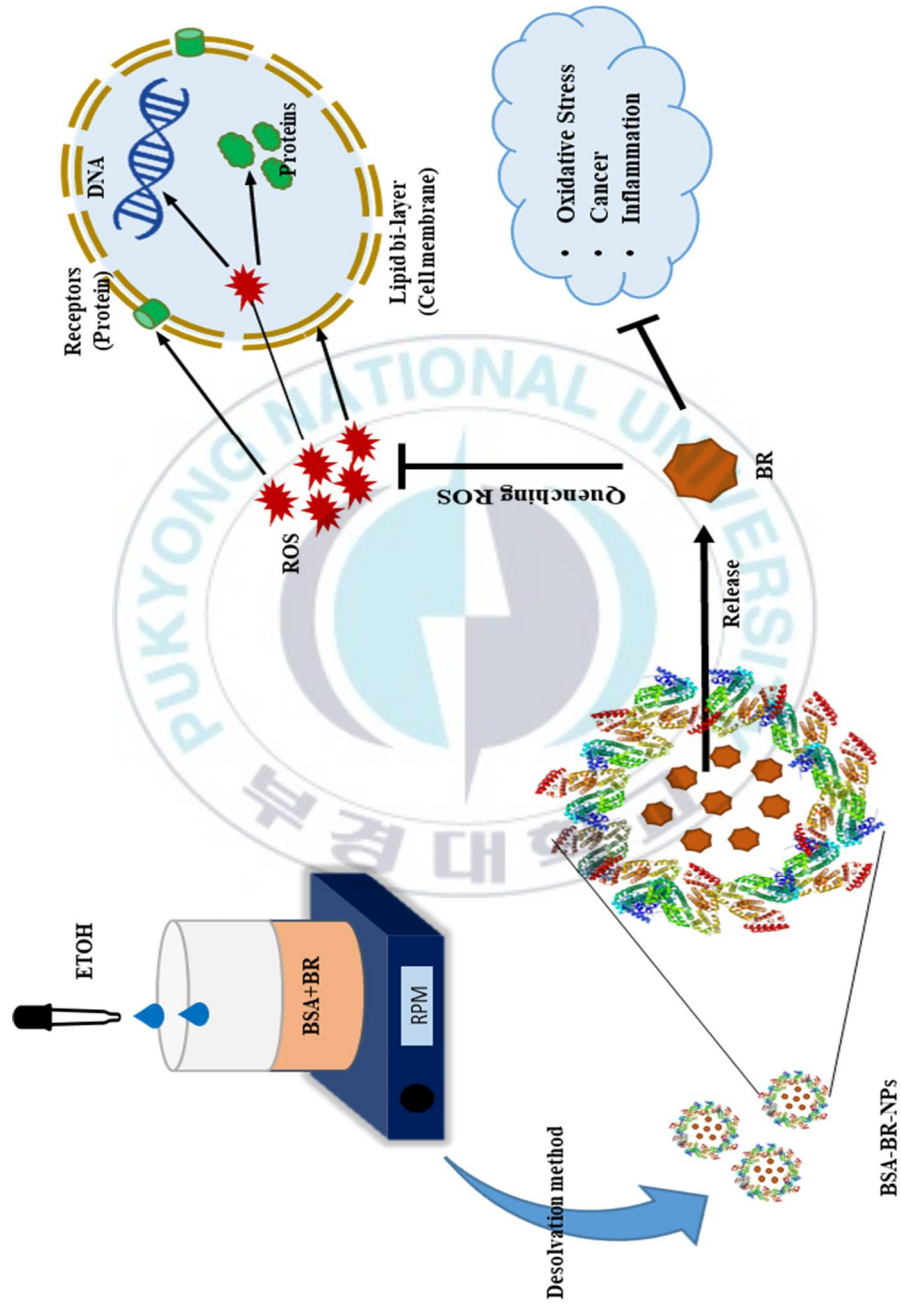


**FIGURE 1: GRAPHICAL ABSTRACT**



## CHAPTER 1: INTRODUCTION



## 1.1. OXIDATIVE STRESS

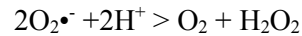
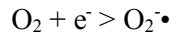
### 1.1.1. OXIDATIVE STRESS AND FREE RADICALS

The production and degradation of undesired secondary oxidants is usually a balanced process in normal life. Oxidative stress is the result of an imbalance between the pro-oxidant and antioxidant systems in favor of the former.[1]

An increase in oxidative stress and/or a reduction in antioxidants leads to oxidative reactions that cannot be prevented or repaired, so that they can alter and modify standard biological components and cause injury, abnormal metabolism, physiological dysfunction, and potentially a disease state.[2, 3]

Oxidative reactions are implicated in numerous diseases and their symptoms, including coronary heart disease, pulmonary disease, diabetes, autoimmune disorders, and cancer, and many more.[2, 4] Molecularly, reactive oxygen species (ROS) are responsible for most of the reactions resulting in oxidative stress.[4]

The body contains a variety of reactive molecules, like OH, ONOO, NO, and ClO. Biologically, ROS can arise from both metabolic processes and from oxygen "activation" by physical irradiation. The main ROS product is superoxide radical anion ( $O_2^-$ ), by which oxidizing and reducing properties are presented. Dismutation depletes superoxide in order to produce oxygen and hydrogen peroxide ( $H_2O_2$ ), a very weak oxidant which attacks mostly thiols.[1]



ROS provides the specific characteristic properties, such as instability and high chemical reactivity. ROS levels play a critical role in its activity. High ROS level increases the oxidative stress response within the cell, causing cell damage through different mechanisms such as protein oxidation, lipid peroxidation via chain reactions in phospholipid bilayers, or DNA damage.[1, 5]

By this means, cells are killed, undergo apoptosis, or accumulate mutations and changes in their metabolism, leading to cancer. This situation will promote the growth of the cancerous cells in the body, resulting in more ROS being generated in the body. These ROS will contribute to the spread of cancer cells and encourage angiogenesis and subsequently increase metastasis potential.[5]

Cancer cells gain an advantage due to the elevated ROS level present in the cancer environment. Falling or raising a specific level of ROS can disrupt the favorable situation for cancer cells. Hence, scavenging ROS could serve as an effective strategy for cancer treatment and angiogenesis prevention. Conversely, ROS in a high enough concentration can also cause cell damage and lead to apoptosis. Therefore, increasing ROS levels in a cancer environment can also be an effective countermeasure against cancerous and abnormal cells.[2, 6]

### 1.1.2. TARGETS OF OXIDATIVE STRESS

Because reactants appear to be highly reactive and have a short half-life, the damage they cause is usually localized near where they are generated. It is known that oxidative damage affects nearly all biological macromolecules, including proteins, membranes, lipids, and DNA (Figure 1.2). [7]

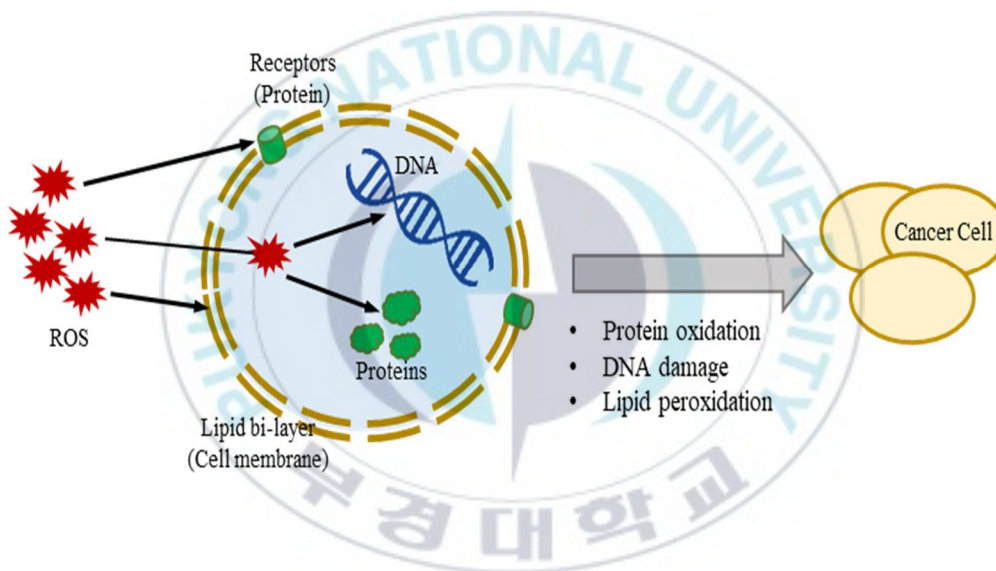


Figure 1.2. Oxidative Stress and ROS mechanism

#### 1.1.2.1 PROTEINS

Proteins are oxidized by ROS through specific mechanisms, including ionizing radiation, simple peptides, and proteins that are exposed to radical-producing conditions.[8] In addition to their relative amount of oxidation-sensitive amino acids,

such as cysteine and methionine residues, their molecular conformation, their localization in the cell, and their degradation rate, certain proteins are more susceptible to oxidative targeting than others. As a result of protein damage during stressful circumstances, proteins may lose structural and functional characteristics, such as the expression of various enzymes, receptors, membrane transporters, and cytoskeletal proteins.[9-11]

#### **1.1.2.2. NUCLEIC ACID**

DNA damage induced by ROS has a characteristic pattern of modification and is chemically and structurally described. DNA damage is a consequence of the generation of hydroxyl radicals, for example, through Fenton chemistry.[12] Almost all DNA molecule elements are known to undergo reactions with hydrogen radicals. There is a direct relationship between mutagenic potential and the number of oxidative DNA lesions that cannot be repaired. The repair mechanisms are known to degenerate with age, leading to an accumulation of DNA lesions. DNA damage sites vary in their DNA sequence specificity, which is related to mutation frequency. Consequently, the study of specific DNA damage sequences would be valuable for cancer prevention.[13, 14]

### 1.1.2.3. MEMBRANE LIPIDS

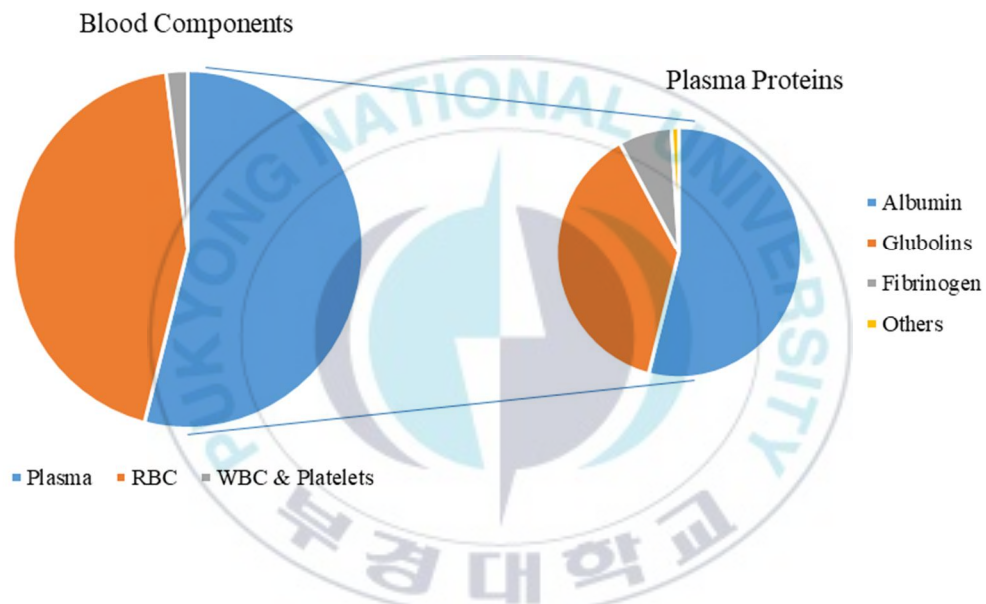
Fluid membranes are crucial for numerous cell functions; even minor changes in membrane fluidity may contribute to abnormal cellular functions. Most of the fluid properties of cells are due to the polyunsaturated fatty acids found within the lipid bilayer. They are the primary targets of reactive oxygen species. They are mainly attacked by OH, which starts the process of lipid peroxidation (LH). [7, 10]



A large amount of lipid peroxidation in a biological membrane results in a loss of fluidity, a decrease in membrane potential, a rise in permeability to H<sup>+</sup> and other ions, and eventual rupture resulting in cell and organelle contents being released. The degenerative process of lipid peroxidation under conditions of oxidative stress is nevertheless responsible for the accelerated aging of people and the development of chronic diseases through the disruption of the lipid packing, which in turn hinders the function of biological membranes.[15, 16]

## 1.2. ALBUMIN

Serum Albumin (SA) is the most abundant protein in plasma, accounting for around 55% of the blood proteins (35-50 g/l in human serum) (Figure 1.3.). [17]



SA is from the homologous proteins family with unique constructive properties and particular ligand-binding features. SA synthesizes by the liver with a non-glycosylated polypeptide chain of 585 amino acids with a size around 7nm and 66.5 kDa molecular weight (Figure 1.4.). [17, 18]

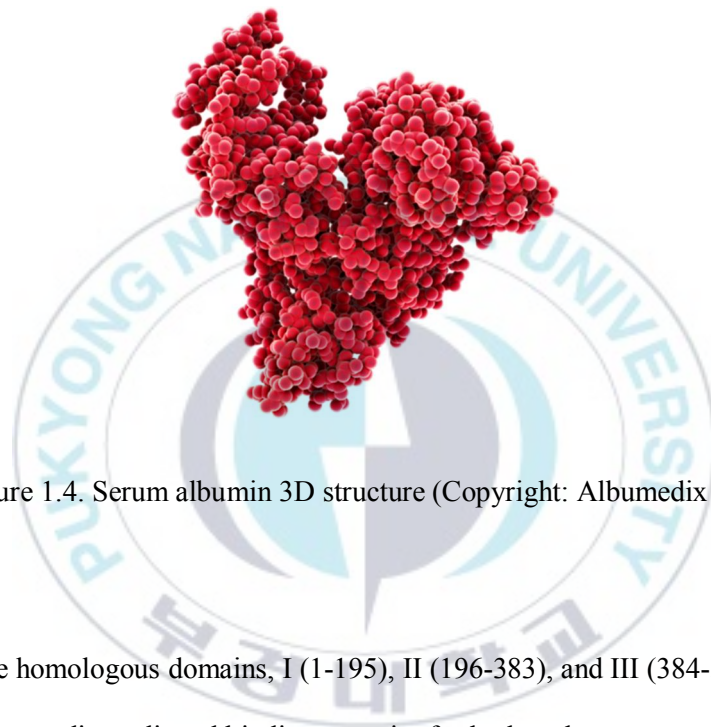


Figure 1.4. Serum albumin 3D structure (Copyright: Albumedix Ltd.)

SA has three homologous domains, I (1-195), II (196-383), and III (384-585), providing extraordinary ligand binding capacity for both endogenous and exogenous compounds (Table 1.1). [19]

Table 1.1. Serum albumin binding sites. [19-21]

Binding site	Location	Ligand	Note
N-terminal	DIA	Co(II), Ni(II), Cu(II)	It consists of three amino acids
Fatty Acid	DI, DII, and DIII	Fatty Acids, Heme, Bilirubin, aromatic carboxylates, heterocyclic anions	FA binding sites
Cys34	DIA	Au(I), Hg(II), Pt(II), and NO	Antioxidant activity, the largest portion of free thiol in plasma
Meta Binding Site	DI, DII	Cu(II), Ni(II), Cd(II), Zn(II)	Surrounded by FA1, FA2, and FA7
Met298	Between DIIA and DIIB	Pt(II)	Antioxidant activity by metal chelating.
Thyroxine	DIIA, DIIIA, and DIIB	Thyroxine (T4)	It consists of 4 binding sites.

SA has a long circulatory half-life through the body, around 21 days. This long circulatory half-life is due to the size of this protein above the kidney filtration threshold and the neonatal Fc receptor (FcRn) mediated recycling property of this compound.[17, 22]

SA is the principal determinant of plasma oncotic pressure and the primary modulator of fluid distribution through the body sections. Besides, SA is the primary carrier for fatty acids, nutrients, metal ions, and drugs through the body and changed their pharmacokinetics and potentials in the body. [23]

The single free thiol Cys34 within domain I acts as a natural binding site for metal ions and a physiological antioxidant, which accounts for 80% of the reduced thiols in human plasma, participating in free radical scavenging like ROS and NO (Figure 1.5.). [24-26]

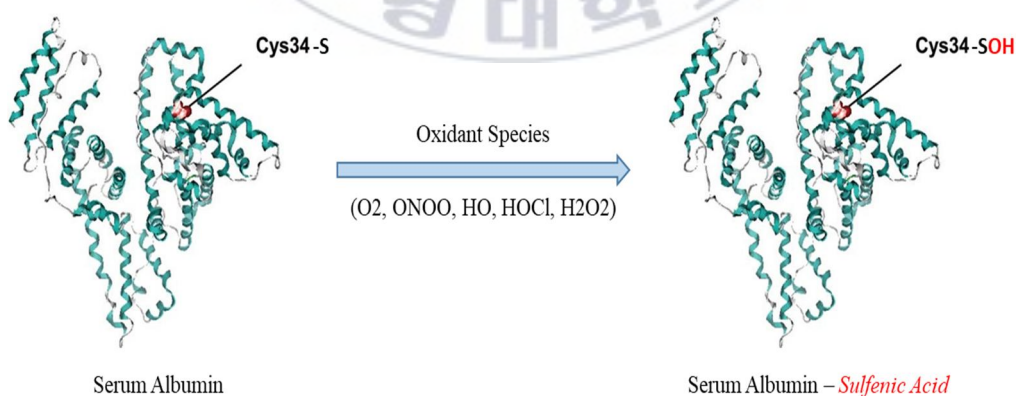


Figure 1.5. Cys34 binding site and antioxidant activity

### 1.3. ALBUMIN NANOPARTICLES

Albumin and albumin nanoparticles are popular drug carriers and drug delivery systems in pharmaceutical sciences due to their biocompatibility, biodegradability, long circulatory half-life, high drug encapsulation capacity, non-immunogenicity, inherent binding capacity, and targeting ability to malignant tissues (Figure 1.6.). [27-29]

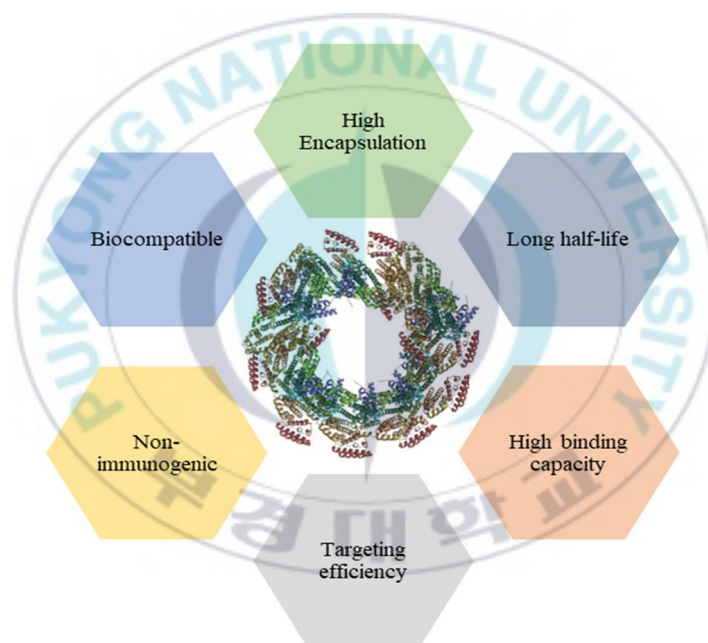


Figure 1.6. Advantages of Albumin nanoparticles

Albumin nanoparticles can deliver a drug inside and/or on the surface to the site of action and accumulate in the tumor environment due to targeting ability, like secreted protein acidic and rich in cysteine (SPARC) and glycoprotein 60 (gp60). [30, 31]

Albumin nanoparticles represent the functions of SA, like antioxidant activity while carrying a therapeutic or a targeting compound, and this can increase their efficiency as a drug carrier. [32]

Albumin nanoparticles are produced by different techniques like high-pressure homogenizer, sonochemical technique, and desolvation. [29, 33, 34]

The desolvation method is a simple, cheap, and reproducible large-scale fabrication method. In this technique, there are two phases, solvent and non-solvent phase, that are usually D.I. Water or PBS and ethanol or acetone, respectively. The addition of the non-solvent phase would lead to form the nanoparticles and has a critical role in nanoparticle size, morphology, and yield (Figure 1.7.). [35-37]

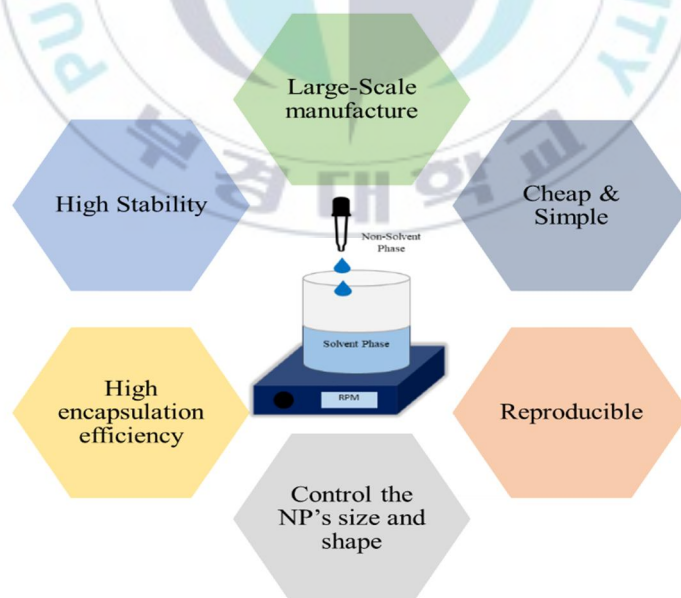


Figure 1.7. Desolvation technique

## 1.4. BILIRUBIN

Bilirubin is an endogenous metabolite produced by the catabolism of heme.

Circulating in the bloodstream, red blood cells typically have a life expectancy of 120 days.[38] As part of the reticuloendothelial system in the spleen and bone marrow, damaged or old red blood cells are phagocytosed and removed from circulation.

Phagocytosis degrades hemoglobin, and heme becomes separated from globin during the process. As globin breaks down, amino acids enter the bloodstream, which is then used for erythropoiesis. Meanwhile, the heme is decomposed by the heme oxygenase (HO) into iron ( $\text{Fe}^{2+}$ ) and biliverdin IX. The iron will reuse for the erythropoiesis, and the hydrophilic biliverdin is reduced by biliverdin reductase into the hydrophobic compound bilirubin (unconjugated bilirubin).

As unconjugated bilirubin is water-insoluble, it circulates in the blood bound to the serum albumin and is transported in plasma from the reticuloendothelial system to the liver. Hepatocytes convert unconjugated bilirubin into water-soluble bilirubin with glucuronic acid (conjugated bilirubin). Then, the conjugated bilirubin is secreted into the bile without any physiologic function in the intestinal tract. Following entering the colon, conjugated bilirubin converts by the colonic bacteria into stercobilin, which is excreted in the feces. While most bilirubin is excreted as stercobilin, a small amount of urobilinogen is reabsorbed into the blood, modified by the kidneys, and excreted in the urine (Figure 1.8).[39-41]

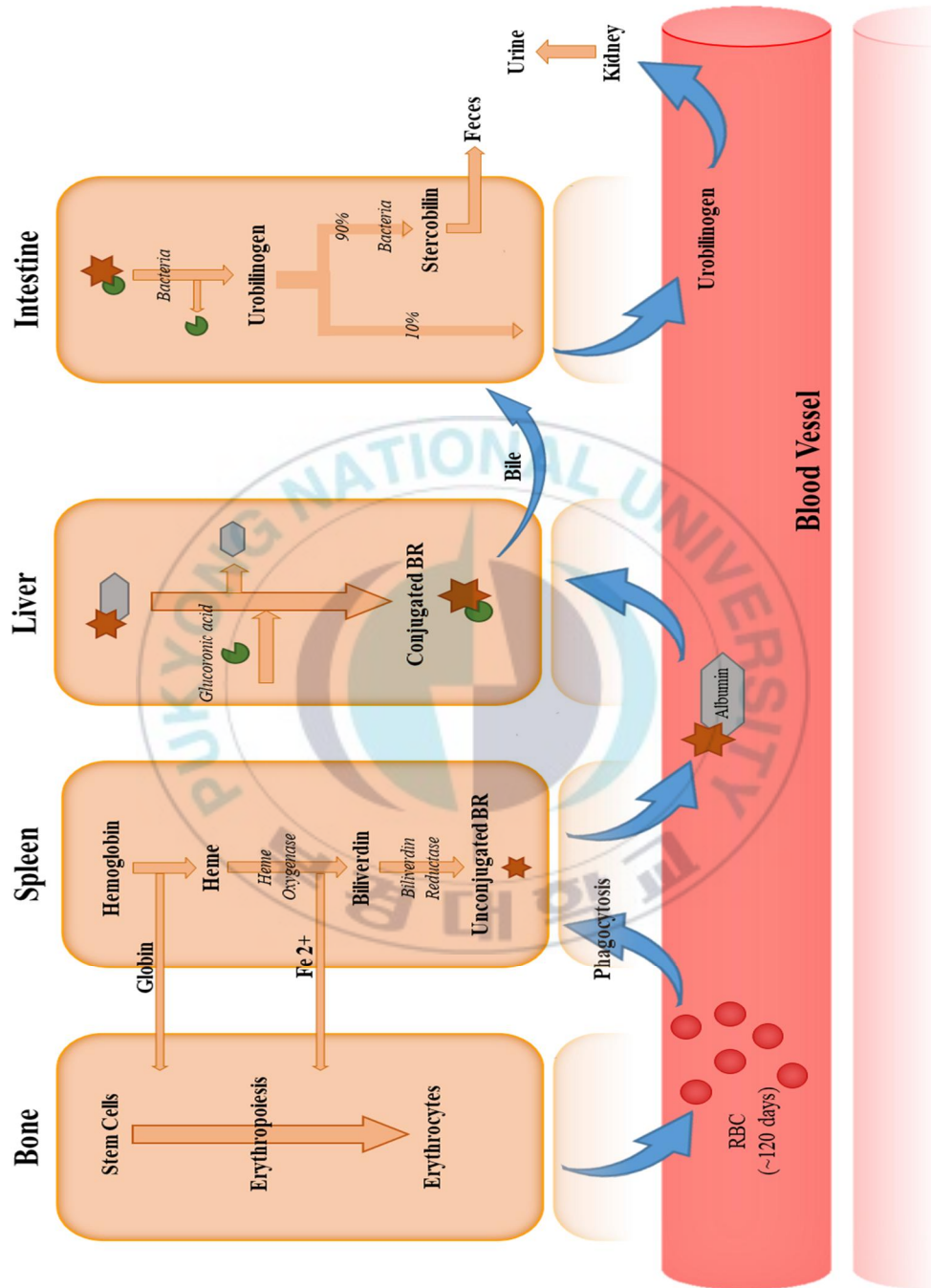
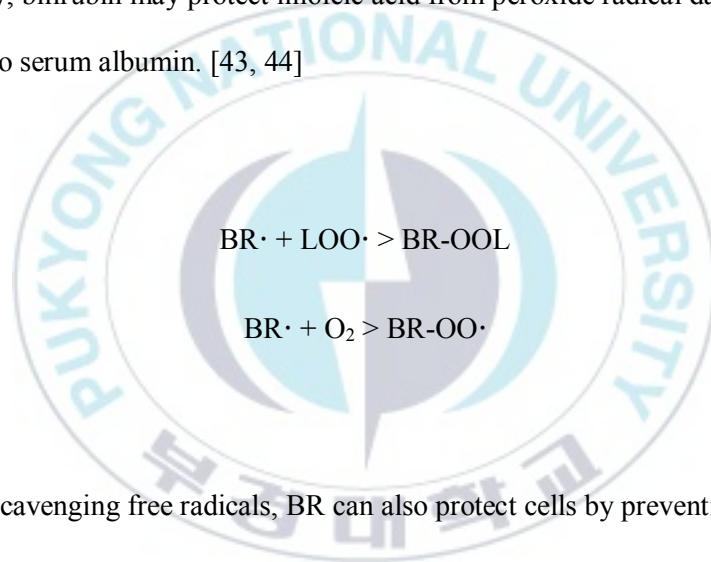


Figure 1.8. Bilirubin metabolism

Bilirubin protects plasma proteins by inhibiting oxidative modifications such as protein fragmentation, tryptophan and tyrosine oxidation, and the production of carbonyl groups.[42]

It can efficiently scavenge a broad range of reactive oxygen species (ROS), can interact with superoxide anions and peroxy radicals, and can be used as a reducing substrate for peroxidases in hydrogen peroxide or organic hydroperoxide.

Additionally, bilirubin may protect linoleic acid from peroxide radical damage when it is bound to serum albumin. [43, 44]



As well as scavenging free radicals, BR can also protect cells by preventing lipid bilayer peroxidation and disruption by scavenging free radicals that make lipid peroxidation chains on the cell membrane.[42, 45]

BR is a lipophilic compound that can pass through cell membranes. BR's major mechanism of toxicity takes place within the cell. The effect of BR on cells results from inhibition of enzyme systems and inhibition of cell regulatory processes, such as protein or peptide phosphorylation, and by these mechanisms, it damages cells. [39, 46, 47]

## 1.5. OBJECTIVES OF THIS STUDY

Bilirubin is a potent protectant against cellular oxidative damage. Despite its well-known anti-oxidative properties, bilirubin is rendered difficult for clinical use because of its water insolubility and rapid clearance in the body. [48, 49]

Albumin is the primary transporter in the blood due to its long circulatory half-life and biocompatibility. Besides, albumin binds to different compounds and can precisely localize in cancer tissues.

In this study, we explored to:

- Provide a simple and scalable fabrication technique for BSA-BR-NPS, synthesis, and characterize them.
- Overcome the water insolubility of BR, protect it from oxidation, and save its therapeutic potentials by encapsulating it in albumin nanoparticles, i.e., BSA-BR-NPS.
- Achieve a sustainable release profile of BSA-BR-NPS, which protects the BR from repaid clearance from the body and optimizes its therapeutic efficiency according to its releasing manner.
- Investigate the anionic and cationic free-radicals scavenging by BSA-BR-NPS and its antioxidant activity.
- Measure the biocompatibility of the BSA-BR-NPS on different normal cells.
- Evaluate the efficacy of BSA-BR-NPS on various cancer cells with respect to the BR loading content.

## CHAPTER 2: MATERIALS



Bovine serum albumin (BSA, 66.4kDa) was purchased from MP biomedical LLC (Ohio, United States of America).

Bilirubin (BR) was gained from Tokyo Chemical Industry Co., Ltd. (Tokyo, Japan).

Ethyl alcohol (ETOH, 99%), Hydrochloric acid (HCL, 1N), Acetone (99%), and Hydrogen peroxide (H<sub>2</sub>O<sub>2</sub>, 35%) were bought from Daejung chemicals and metals Co., Ltd. (Gyeonggi, South Korea).

N-(3-Dimethylaminopropyl)-N-ethyl carbodiimide hydrochloride (EDC), McCoy's 5A Medium, MTT Formazan, and dialysis tubes (molecular weight cut off = 12000 Da) were obtained from Sigma-Aldrich (Steinheim, Germany).

Sodium hydroxide (NaOH, 1M) was obtained from Samchun Chemical Co., Ltd. (Gyeonggi, South Korea).

Trypsin-EDTA was purchased from Gibco, Thermo Fisher Scientific Co., Ltd. (South Korea).

## CHAPTER 3: EXPERIMENTS



### 3.1. NANOPARTICLES PREPARATION

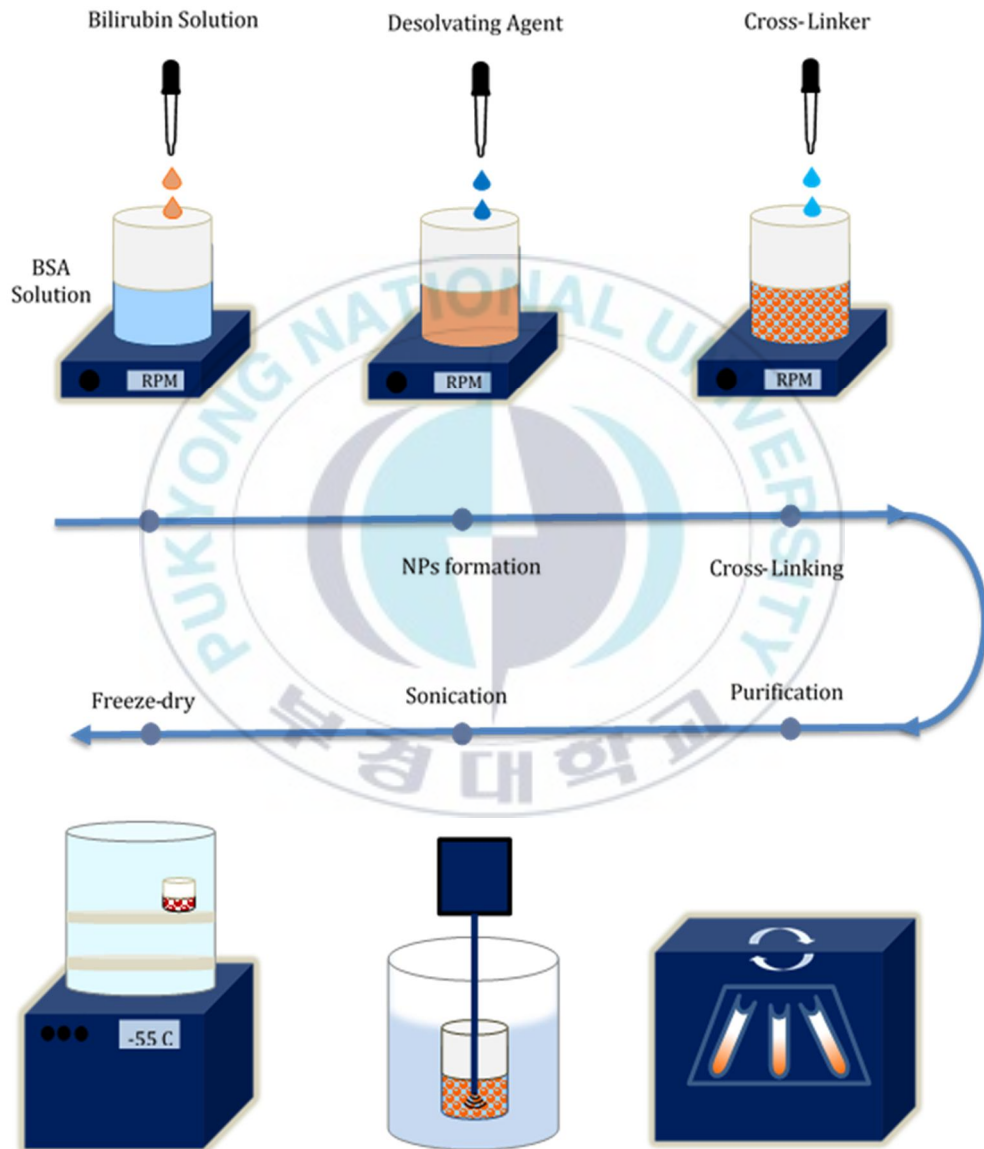


Figure 3.1. Nanoparticles preparation process

### **3.1.1. NAKED-BSA NANOPARTICLES (BSA-NPS)**

The preparation of BSA nanoparticles was performed according to the modified desolvation technique. First, 200 mg of BSA powder weighed and dissolved in 4 mL of deionized water. After that, 8 mL anhydrous ethanol was added to the BSA solution (50 mg/mL D.I. Water) using a syringe pump drop-wise at a rate of 2 mL/min, at room temperature under constant stirring (1200 rpm and using 1 cm magnet). The turbidity in the solution illustrates the BSA nanoparticle formation. After 10 min of constant stirring, 0.5 mL EDC (52 mM) solution was added to the nanoparticles mixture ends up with approximately 0.41 mg/mL (2.2 mM) working concentration to cross-link all the amino acid residues and stabilize the nanoparticles. The mixture was further stirred overnight to obtain a uniform cross-linked nanoparticle solution (Figure 3.1.).

### **3.1.2. BR-LOADED BSA NANOPARTICLES (BSA-BR-NPS)**

To prepare BR-loaded BSA nanoparticles modified desolvation technique was performed. At first, 200 mg of BSA powder was dissolved in 4 mL of deionized water. BR solution was made by dissolving BR powder in NaOH 0.1 M solution with a 10 mg/mL concentration in a light-controlled condition (in a foil-wrapped beaker and a dark room). After that, 1mL fresh BR solution (10 mg) was added to the BSA solution (50 mg/mL). Then, 1 mL HCl 1 N was added to the mixture drop-wise until the pH of the solution reaches pH 6~7 (Figure 3.2.).

After that, 8 mL anhydrous ethanol was added to the BSA-BR solution using a syringe pump drop-wise at a rate of 2 mL/min, at room temperature under constant stirring for 30 min (1200 rpm and using 1 cm magnet) in a light controlled situation. The turbidity in the solution illustrates the BSA-BR nanoparticle formation. After 10 min of constant stirring, 0.5 mL of EDC (52 mM) solution was added to the nanoparticles mixture ends up with approximately 0.41 mg/mL (2.2 mM) working concentration to cross-link all the amino acid residues and stabilize the nanoparticles. The mixture was further stirred overnight to obtain a uniform cross-linked nanoparticle solution.

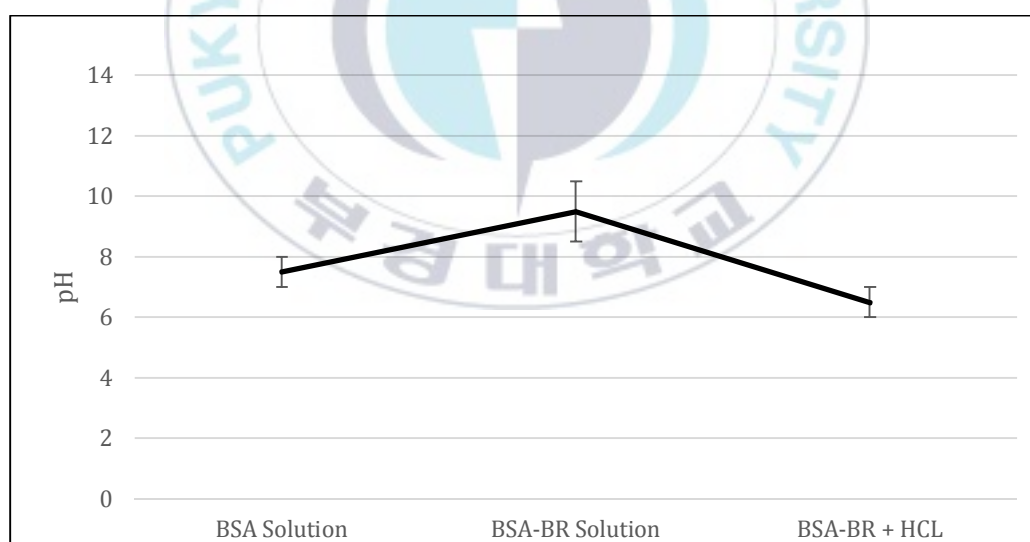


Figure 3.2. pH adjustment in BSA-BR-NPS preparation process

### 3.1.3. NANOPARTICLES PURIFICATION

The final BSA-NPs and BSA-BR-NPs suspension were purified using ultracentrifuge (1580-R, Labogene, South Korea) at 12000 rpm for 15 min at 25 °C for three times by redispersing the nanoparticles pellet in 12 mL of deionized water to ensure removing the ethanol, and free BSA, BR, and EDC from the nanoparticles solution. The supernatant after centrifugation was collected each time, and the absorbance of both Free-BSA and Free-BR were measured by UV-spectrophotometry technique (Biodrop). The Free-BSA (MW = 66,400 daltons, the molar extinction coefficient at 280 nm is approximately  $43,824 \text{ M}^{-1}\text{cm}^{-1}$ ), and Free-BR (MW = 584.7 daltons, the molar extinction coefficient at 460 nm is approximately  $53,846 \text{ M}^{-1}\text{cm}^{-1}$ ) concentrations were calculated according to the Beer-Lambert law and the standard calibration of BR in NaOH 0.1 M ( $Y = 3.3499X - 0.0601$ ,  $R^2 = 0.9986$ ). After centrifugation, the pellet at the bottom redispersed in 12 mL of D.I. Water by pipetting and vortexing. The suspension was sonicated with probe sonication (BKUP-250N, Korea process technology, South Korea) with 50% power for 5 min at 4 °C to get a homogenous nanoparticle solution. After that, the nanoparticle solution was freeze-dried (GZ-HC3110-CHR, Gyrozen, South Korea) for 48 hr at -55 °C to obtain a fine powder form of nanoparticles. The final, dried BSA-NPs and BSA-BR-NPs were weighted and stored at -20 °C before usage.

## **3.2. NANOPARTICLES OPTIMIZATION**

In order to optimize the nanoparticles produced with the desolvation method and obtain the highest nanoparticle yield with an acceptable mean size, different criteria were considered, such as the size, stability, and yield% of each synthesis to determine the optimum yield of the nanoparticles with an acceptable size.

### **3.2.1. SOLVENT/NON-SOLVENT RATIO**

The BSA-NPs formed when the non-solvent was added to the solvent containing. The solvent/non-solvent ratio was applied to the nanoparticles process to optimize the highest yield % and an acceptable size after NPs formation. The non-solvent phase was added with a rate at 2 mL/min to the solution with the solvent to the non-solvent ratio of 1:1, 1:2, 1:2.5, and 1:3. After the NPS formation and purification, the size and yield % of each batch were measured.

## **3.3. NANOPARTICLES CHARACTERIZATION**

### **3.3.1. YIELD%**

To calculate the yield of the synthesized nanoparticles, the Free-BSA (MW = 66,400 daltons, the molar extinction coefficient at 280 nm is approximately  $43,824 \text{ M}^{-1}\text{cm}^{-1}$ )

in the supernatant after nanoparticles purification was measured by the UV-spectrophotometry method according to equation 1.

$$\text{Equ. 1. Nanoparticles Yield \%} = (\text{total BSA} - \text{Free BSA}) / \text{total BSA} * 100$$

### **3.3.2. SIZE**

To measure the size of the nanoparticles, 1 mg of BSA-NPs and BSA-BR-NPs was dispersed in 1 mL of deionized water and sonicated for 2 min in an ice bath. After that, the average size and polydispersity index (PDI) were measured using dynamic light scattering (DLS) with a Litesizer-500 (Anton Paar, Austria) from three separate runs according to the measurements taken from different NPs batches.

### **3.3.3. STABILITY**

To measure the stability of the lyophilized powder of BSA-NPs and BSA-BR-NPs, 1 mg of the nanoparticles was dispersed in 1 mL of deionized water by sonication for 2min in an ice bath. The size of the nanoparticles was measured using DLS on the days 0, 1, 2, 3, 7, 10, 14, 21, 28, and 35, respectively, to determine the time-dependent stability of the nanoparticles.

### **3.3.4. ZETA POTENTIAL**

To measure the nanoparticle's zeta potential, 1 mg of BSA-NPs and BSA-BR-NPs powder was first dispersed in 1 mL deionized water and sonicated for 2 min in an ice

bath. Second, the zeta potential of the naked-NPs and drug-encapsulated nanoparticles were measured using DLS. Three runs from each sample were implemented.

### **3.3.5. MORPHOLOGY**

The morphologies of the prepared NPs, such as sphericity and aggregation, were examined using scanning electron microscopy (SEM, MIRA 3, Tescan, Czech Republic). Lyophilized NPs in the powder form was coated with Platinum under vacuum before SEM analysis.

The superficial structure and shape of the NPs were studied using Transmission Electron Microscopy (TEM, JEM-2100F, Jeol, Japan) as well. A drop of the diluted sample was deposited onto a carbon-coated copper grid. The excess sample was removed after 2 min using filter paper. Then, the sample was negatively stained with uranyl nitrate 1% w/v and removed by filter paper after 1min. Finally, the carbon grid was dried at RT, followed by TEM analysis.

### **3.4. BILIRUBIN AND BILIVERDIN CALIBRATION**

The calibration curve of bilirubin and the oxidized form, biliverdin, were obtained by using UV-spectrophotometer (bio drop). A dilution series of BR were prepared by dissolving BR powder in NaOH 0.1 M at 1, 0.9, 0.8, 0.7, 0.6, 0.5, 0.4, 0.3, 0.2, 0.1, 0.09, 0.08, 0.07, 0.06, 0.05, 0.04, 0.03, 0.02, 0.01, and 0.005 mg/mL concentration.

Then, the absorbance of each concentration was measured three times quickly at 440 nm, and the calibration curve and the calibration equation were obtained to calculate D.L% and EE%.

To measure the biliverdin standard curve, the BR dilution series were oxidized at room temperature overnight by adding 0.1 mL H<sub>2</sub>O<sub>2</sub> 0.1 M to each tube. The color changed overnight from orange to green, and no absorbance at 440 nm confirmed the oxidation of BR. After that, the absorbance of each sample was measured at 660 nm 3 times, and the calibration curve and the calibration equation were obtained to use in release assay analysis.

### **3.5. DRUG ENCAPSULATION**

#### **3.5.1. ABSORBANCE**

Successful drug-encapsulation inside the BSA Nanoparticles was confirmed by the UV-spectrophotometer. The absorbance of the Free-BSA, Free-BR, Naked-BSA-NPs, and BSA-BR-NPs was measured by bio drop using Quartz cuvette from 200 nm to 700 nm. The maximum absorbance of BSA and BSA-NPS is at 280 nm, which is related to its protein nature. The BR maximum absorbance appeared at 440 nm that is related to the benzene groups in its chemical structure.

Then, the wave-scans of free-drugs, encapsulated-nanoparticles, and naked-nanoparticles were compared to determine the presence of the drug inside the nanoparticles.

### **3.5.2. ENCAPSULATION EFFICIENCY and DRUG LOADING**

The drug loading and encapsulation efficiency were calculated by equ.2 and equ.3, respectively.

The amount of free drug after NPS purification was considered during the calculation of the drug loading and encapsulation efficiency.

$$\text{Equ.2.: drug loading}\% = ((\text{Total BR} - \text{Free BR}) / \text{Total NP weight}) * 100$$

$$\text{Equ.3.: encapsulation efficiency}\% = ((\text{Total BR} - \text{Free BR}) / \text{Total BR}) * 100$$

### **3.6. RELEASE ASSAY**

To simulate the in vivo bilirubin release profile from BSA-BR-NPs, the experiment was conducted in two different environments by dialysis method. A dialysis tube was selected based on the molecular weight of bilirubin (0.585 kDa) and BSA (66.5 kDa).

BSA-BR-NPs (1 mg/mL, 10% BR loading) were added into the dialysis tubes (MWCO=12 kDa). Then, the tubes were dialyzed against different releasing mediums, PBS (80 mL, pH 7.4, 37 °C), while constant stirring at 120 RPM to simulate the normal in vivo condition, and PBS (80 mL, pH 5.4, 42 °C) plus hydrogen peroxide (H<sub>2</sub>O<sub>2</sub>, 0.1 M) while stirring at 200 RPM to stimulate ROS inflammation in vivo environment (Figure 3.3.). After that, 1 mL of the released medium was collected, and the same volume of fresh medium was supplemented at each predetermined time point (0.5, 1, 2, 3, 4, 6, 10, 20, 24, and 48 h). The released BR from the NPs was oxidized due to the ROS environment and the oxygen in the air, so the samples' absorbance was measured by UV-spectrophotometer at 660 nm to determine the amount of the released drug according to the biliverdin standard calibration curve and equation. The cumulative release of the drug from the NPS was measured by collecting the released amount at each time point.

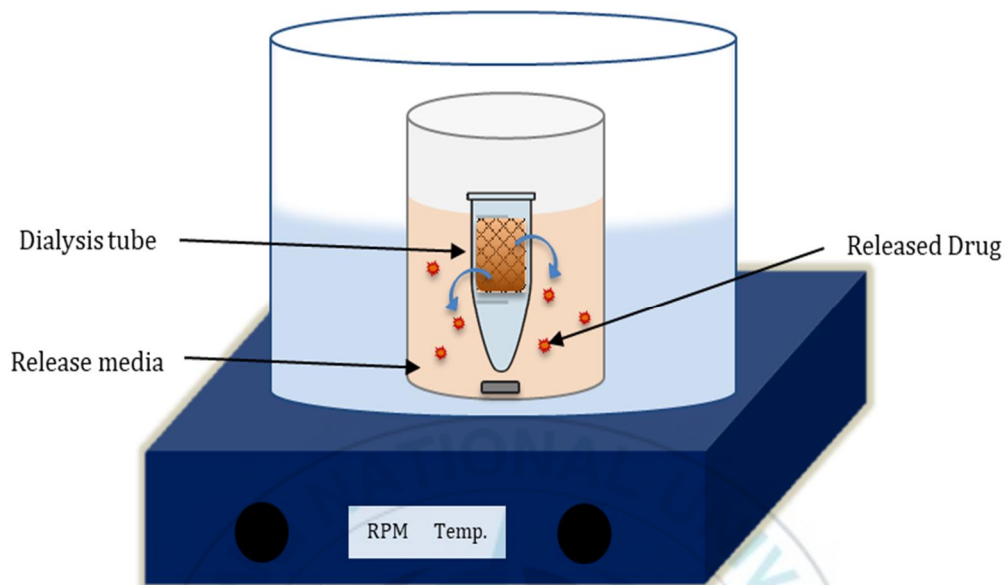


Figure 3.3. BR release assay from BSA-BR-NPs

### 3.7. FREE-RADICAL SCAVENGING

#### 3.7.1. DPPH FREE-RADICAL SCAVENGING ACTIVITY

To measure the anionic free-radical scavenging activity of the BSA-NPs and BSA-BR-NPs, we used the DPPH method. The BSA-NPs and BSA-BR-NPS were diluted to concentrations of 21.37, 42.75, 85.5, and 171  $\mu$ M and were mixed with the DPPH solution (in methanol) in a 96-well plate. After that, incubated 30min at room temperature, and subsequently, the absorbance was recorded at 517 nm.

### **3.7.2. ABTS FREE-RADICAL SCAVENGING ACTIVITY**

To measure the cationic free-radical scavenging activity of the BSA-NPs and BSA-BR-NPs, we used the ABTS method. ABTS solution was prepared by mixing 7 mM ABTS with  $K_2S_2O_8$  2.6 mM, 16 h in the dark condition, and then diluted with the PBS (absorbance value of 0.7-0.73 nm). The BSA-NPs and BSA-BR-NPS were diluted to concentrations of 21.37, 42.75, 85.5, and 171  $\mu$ M and mixed with the ABTS solution in a 96-well plate and incubated 10min at room temperature subsequently the absorbance was recorded at 734 nm.

### **3.8. CELL ASSAY**

For investigating the in-vitro cellular efficiency of the BSA-BR-NPs, and its toxicity on normal and cancer cells, a variety of normal and cancerous cells from different origins were cultured. The cells were supplemented at 37 °C in an incubator under 5% CO<sub>2</sub> conditions for the later experiments.

#### **3.8.1. MTT ASSAY**

To measure the degree of cell viability, an MTT assay was performed. Different cells were seeded in 96-well plates at a density of  $1.5 \times 10^4$  cells/well. After that, the cultures were incubated for 24 h at 37 °C in an incubator.

The cells were treated with Free BR, naked BSA-NPs, and BSA-BR-NPs at 0, 42.75,

85.50, 171.00, 256.51  $\mu\text{M}$  with respect to the amount of BR encapsulation, for 24 h or 48 h at 37 °C. After that, MTT was added to each well for an additional 2 h at 37 °C. Then the medium was discarded, and DMSO (100  $\mu\text{l}$ ) was added to each well. Finally, the absorbance was measured at 570 nm by SYNERGY HTX (Biotek), and the relative cell viability was calculated and compared with the control group.

#### **3.8.1.1 NORMAL CELLS**

Different normal cell lines were treated with free-BR, naked BSA-BR-NPs, and BSA-BR-NPs to investigate the compounds' side effects and biocompatibility and toxicity on normal cells in the body by using MTT assay. The CCD18-co (human normal colon fibroblast cells), BEAS-2B (human non-tumorigenic lung epithelial cells), and NHA (human normal astrocyte cells) cell lines were treated by 0, 42.75, 85.50, 171.00, 256.51  $\mu\text{M}$  of samples w.r.t. BR concentration. And then, the cell viability and the toxicity of the formulations on these cells were calculated by spectrophotometry using SYNERGY HTX (Biotek) and compared with the control group.

#### **3.8.1.2. CANCER CELLS**

The efficiency of the compounds on cancer cells was investigated by treating the cancerous cell lines with free-BR, naked BSA-BR-NPs, and BSA-BR-NPs using MTT assay. The DLD-1 (colorectal adenocarcinoma cells), LN229 (human brain

glioblastoma cells), SKOV-3 (ovarian cancer cells), CAOV-3 (primary ovarian cancer cells), HT-29 (colon cancer cells), SW480 (colon cancer cells), and HCT116 (colorectal adenocarcinoma cells) cell lines were treated by 0, 42.75, 85.50, 171.00, 256.51  $\mu$ M of samples w.r.t. BR concentration. And then, the cell viability and the toxicity of the formulations on cancerous cells were evaluated by spectrophotometry using SYNERGY HTX (Biotek) and compared with the control group.



## CHAPTER 4: RESULTS



#### 4.1. NANOPARTICLES PREPARATION AND OPTIMIZATION

The BSA nanoparticles were prepared by the simple desolvation method as described before. The optimized condition was selected by changing the Solvent: Non-solvent ratio concerning the mean size and yield of the nanoparticles (Table 4.1.). The nanoparticles prepared by the S: NS ratio of 1:2 had the highest yield, around 75%, according to the free BSA absorbance after purification. The size of nanoparticles with the ratio of 1:1, 1:2, 1:2.5, and 1:3 were 92, 122, 143, and 110 nm, respectively. The preparation process with an S: NS ratio of 1:2 had the highest yield and acceptable mean size among the other conditions and was chosen for the rest of the process.

Table 4.1. NPS optimization, Solvent: Non-Solvent ratio

S:NS	1:1	1:2	1:2.5	1:3
Mean Size (nm)	92	122	143	110
Mean Yield%	48	75	63	51

#### 4.2. NANOPARTICLES CHARACTERIZATION

The BSA-NPS and BSA-BR-NPS were characterized after preparation. The nanoparticles' yield was measured using UV-Spectrophotometer by the free amount

of BSA in the supernatant after NPS purification (Table 4.2.). The BSA-NPS yield was 75%, and the BSA-BR-NPS yield was around 67% after purification.

Table 4.2. NPs characterization, Yield %

Formulation	Initial BSA (mg)	Free BSA (mg/mL)	Total Volume (mL)	Yield %
BSA-NPS	200	12.5	12	75
BSA-BR-NPS	200	11.1	13	67

The nanoparticle's mean size, polydispersity index (Pdl), and zeta potential were measure by DLS. 1 mg of NPS powder dispersed in D.I.Water and then analyzed with DLS (Table 4.3.).

Table 4.3. NPs characterization, Dynamic Light Scattering

Formulation	Mean Size (nm)	Mean Pdl	Mean Zeta Potential (m.V)
BSA-NPs	122	0.050	-28.92
BSA-BR-NPs	164	0.204	+21.32

The mean size of the BSA-NPS was 122 nm after preparation (Figure 4.1.). The BSA-NPS mean zeta potential was slightly negative, around -28.92 mV after preparation (Figure 4.2.).

The BSA-NPS were stable during the time, and their mean size after 35 days were 132 nm, which is only 10nm different from the first measurement at day 0 (Figure 4.3.).

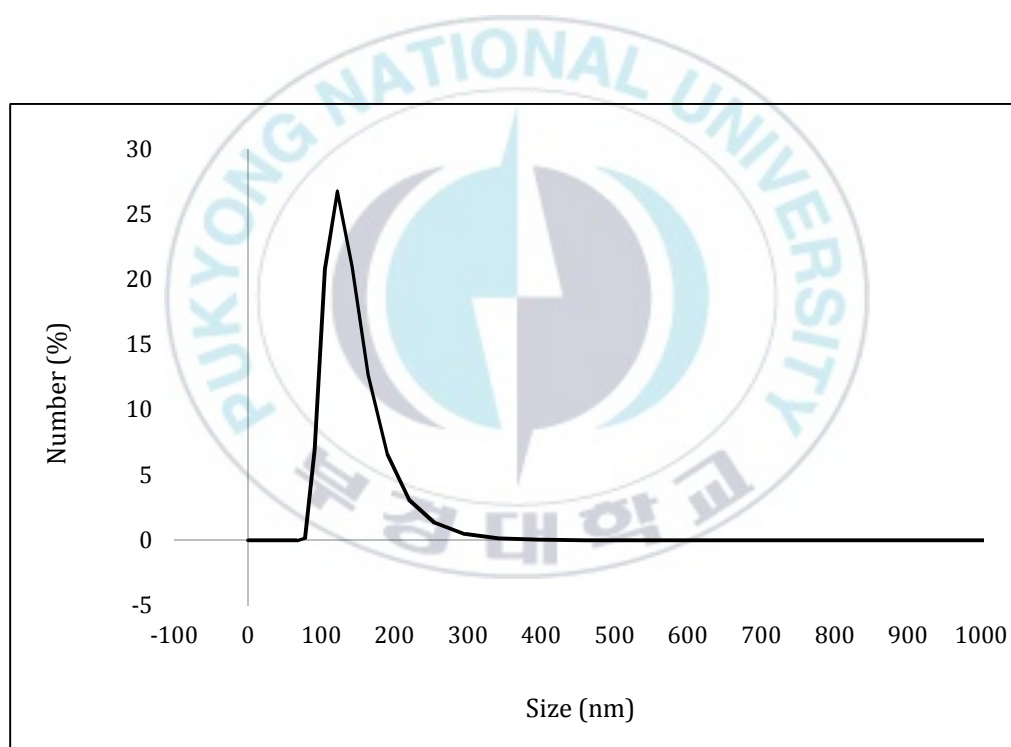


Figure 4.1. BSA-NPs characterization, Size

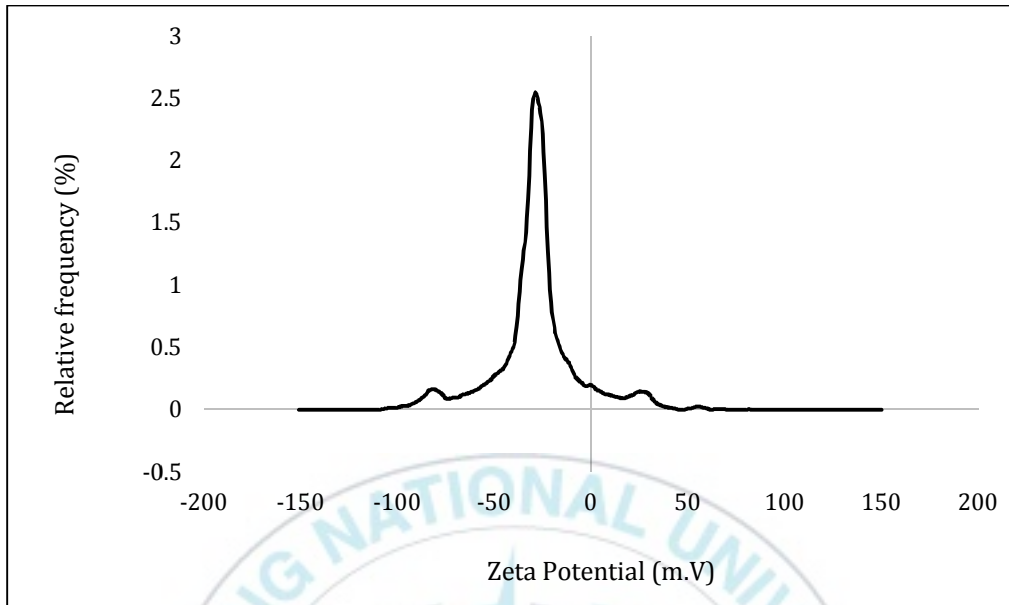


Figure 4.2. BSA-NPs characterization, Zeta Potential

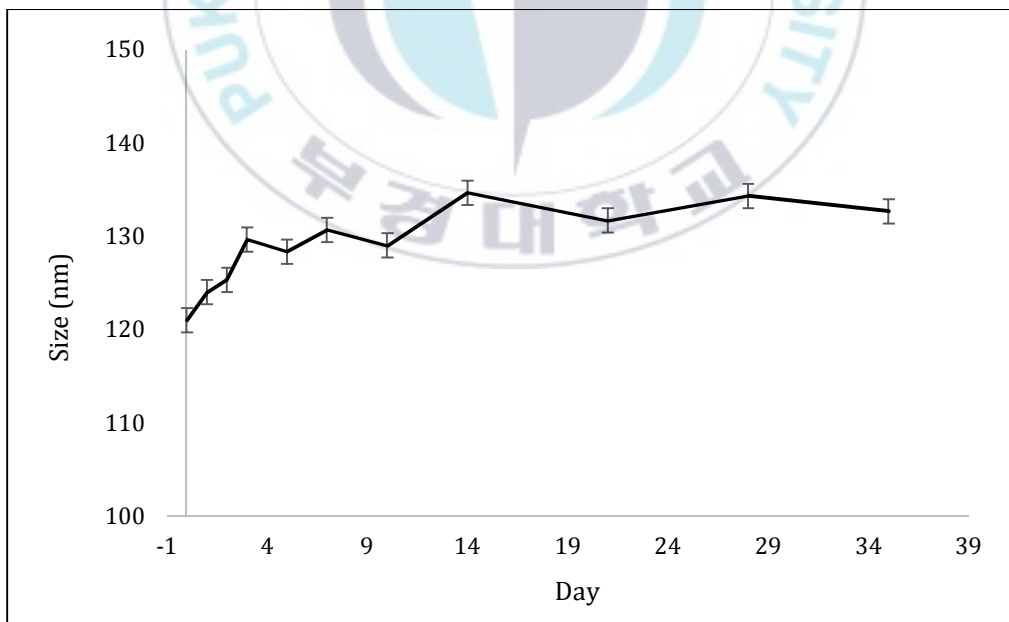


Figure 4.3. BSA-NPs characterization, Size Stability

The BSA-BR-NPS size after preparation was 164 nm (Figure 4.4.). Furthermore, the zeta potential of BSA-BR-NPS became slightly positive after drug encapsulation and was +21.32 mV (Figure 4.5.).

The nanoparticles' stability was observed by their size mean variation of three different batches during 35 days after preparation.

The size of the BSA-BR-NPS showed a stable trend during 35 days and changed less than 10 nm, from 164 nm to 173 nm after five weeks (Figure 4.6.).

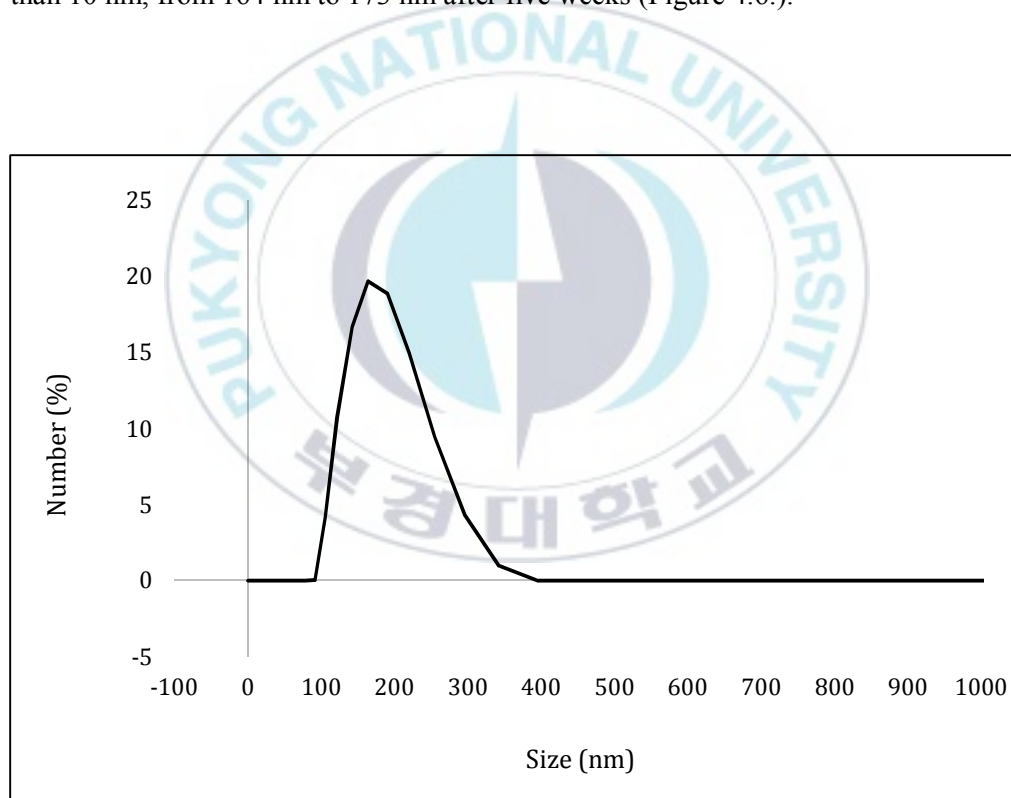


Figure 4.4. BSA-BR-NPs characterization, Size

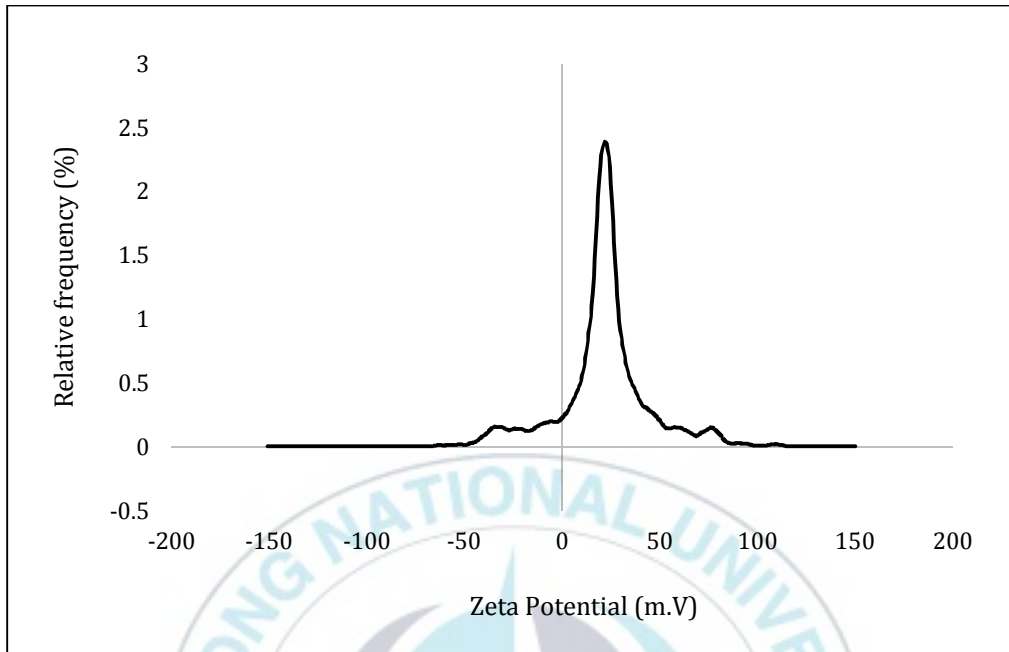


Figure 4.5. BSA-BR-NPs characterization, Zeta Potential

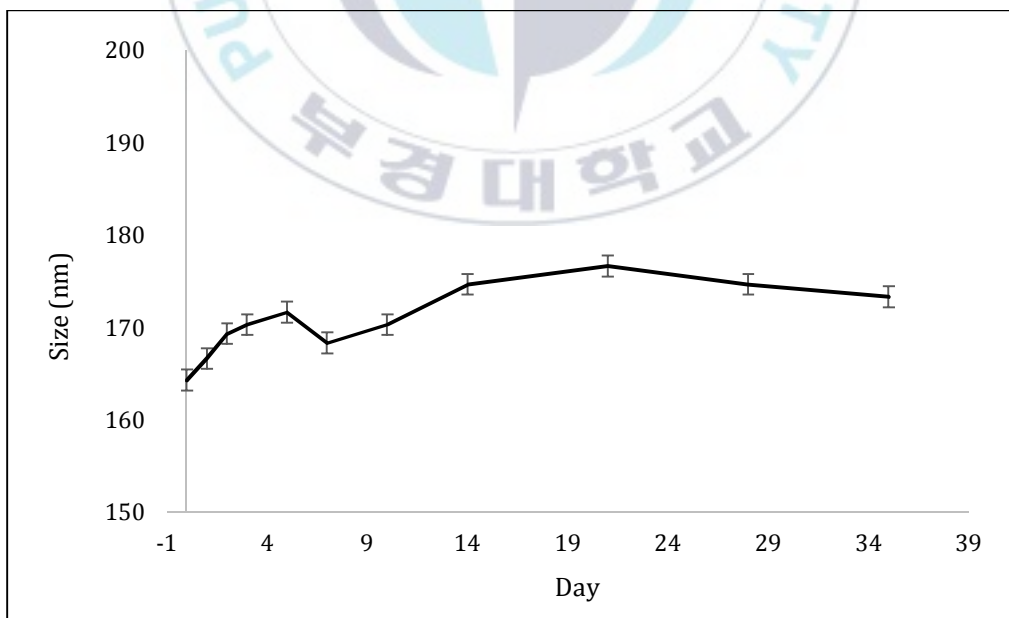


Figure 4.6. BSA-BR-NPs characterization, Stability

The nanoparticles' morphology was characterized by Transmission and Scanning Electron Microscopy (TEM and SEM).

The nanoparticles were loaded on carbon grids and stained with uranyl nitrate, and then dried, and the images took from them by TEM. The BSA-NPS (Figure 4.7.) and BSA-BR-NPS (Figure 4.8.) showed a spherical shape and size less than the DLS measurement. The reason for this size difference is that the NPS is at their most compact form under the microscope rather than the solution phase analyzed by DLS.

To take the SEM photos from the surface of the NPS and observe their aggregation, shape, and morphology, the NPS powders were coated on a holder and coated by a layer of platinum, and then the images took with SEM.

Both BSA-NPS (Figure 4.9.) and BSA-BR-NPS (Figure 4.10.) had spherical shapes and a smooth surface with the same size around 122 nm and 164 nm for BSA-NPS and BSA-BR-NPS, respectively.

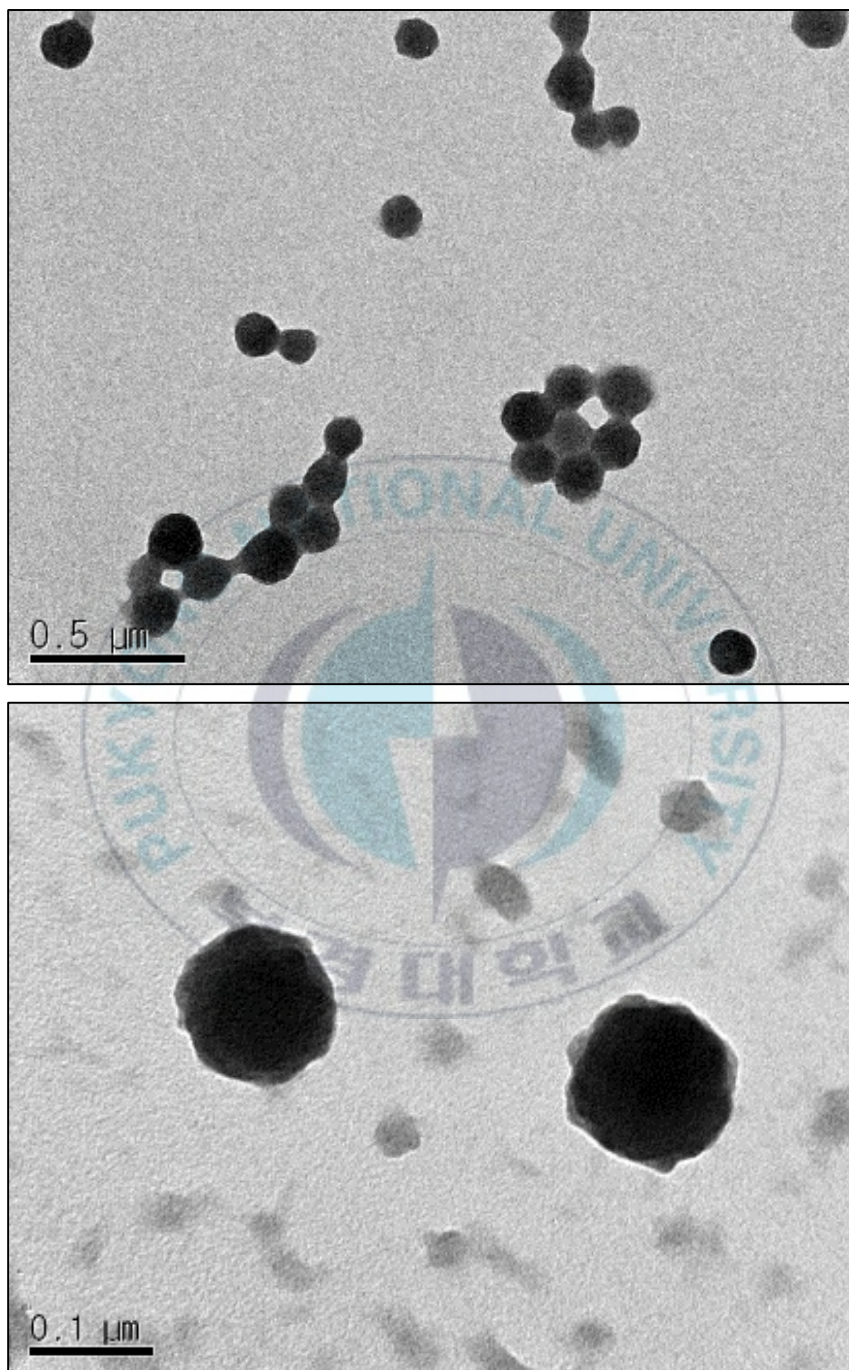


Figure 4.7. BSA- NPs characterization, TEM

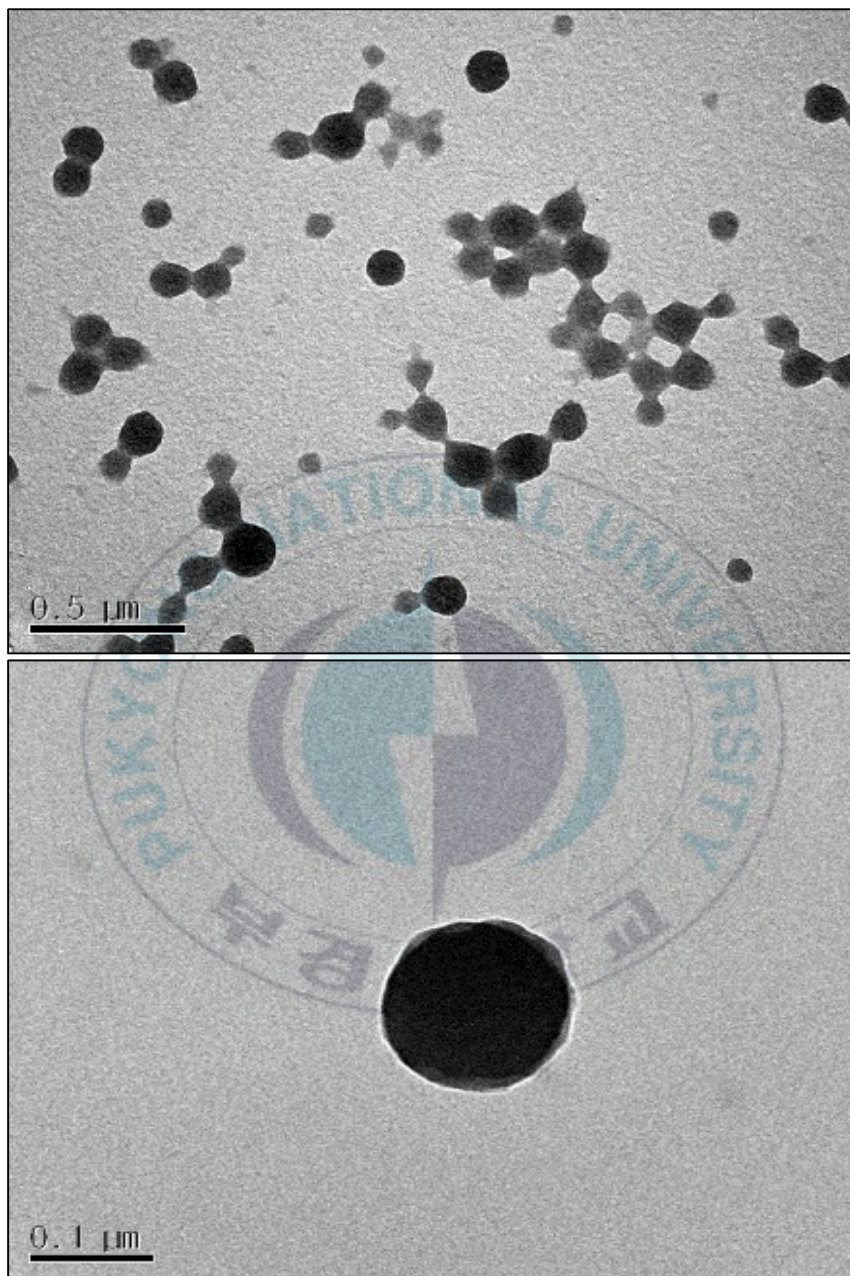


Figure 4.8. BSA- BR-NPs characterization, TEM

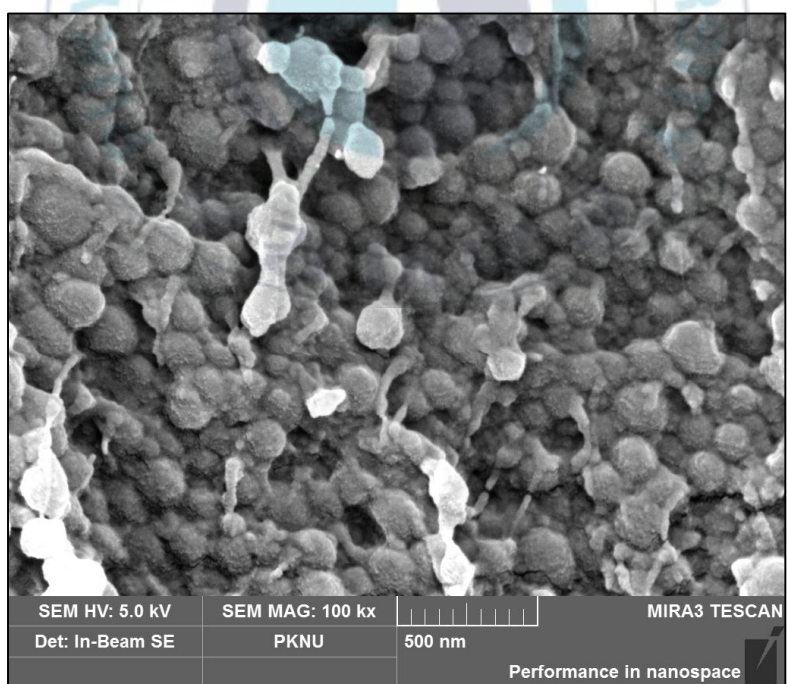
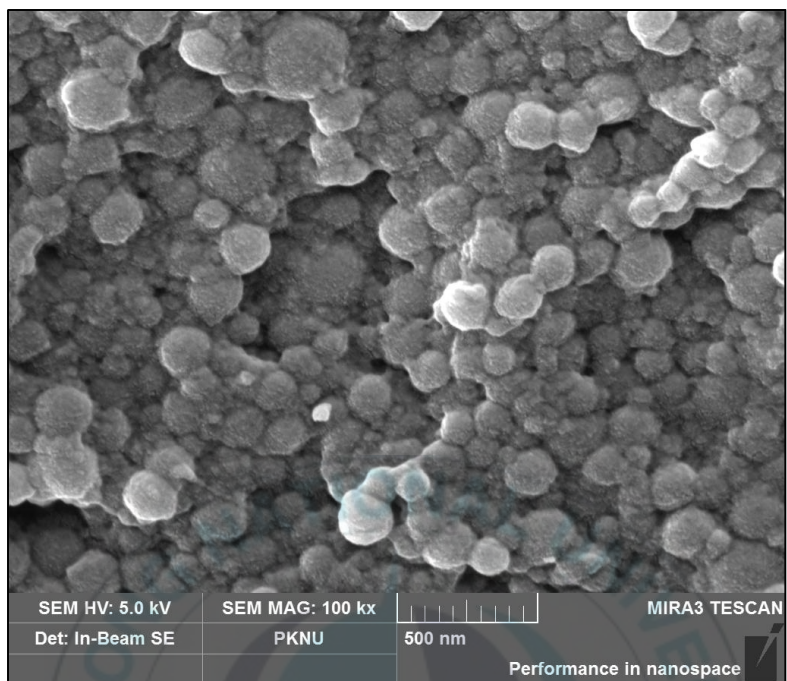


Figure 4.9. BSA-NPs characterization, SEM

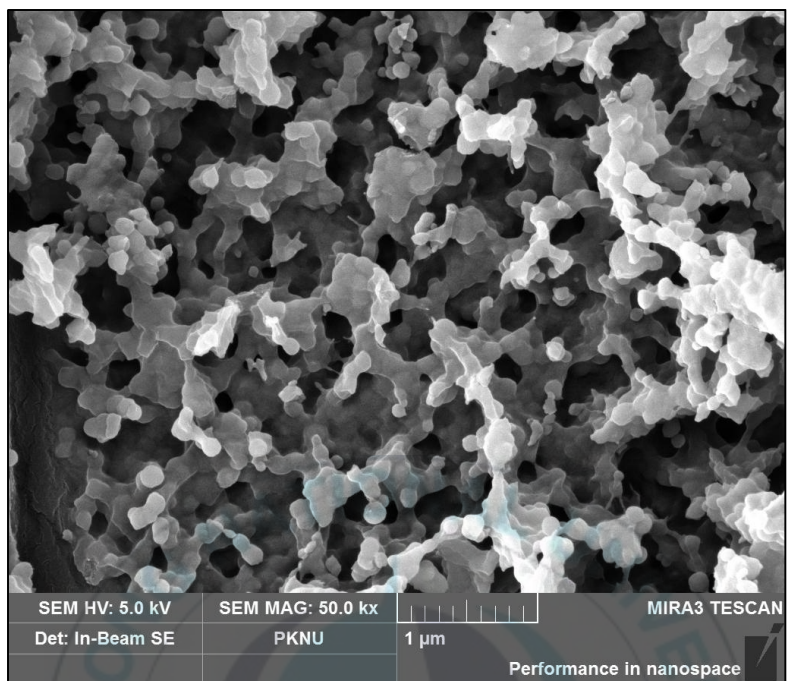


Figure 4.10. BSA-BR-NPs characterization, SEM

### 4.3. STANDARD CALIBRATION

The standard calibration of bilirubin and biliverdin was calculated by preparing a serial dilution from 0.005 mg/mL to 1 mg/mL bilirubin in NaOH. Then the absorbance of each dilution was measured at 440 nm to calculate the standard curve and formula of BR (Figure 4.11.).

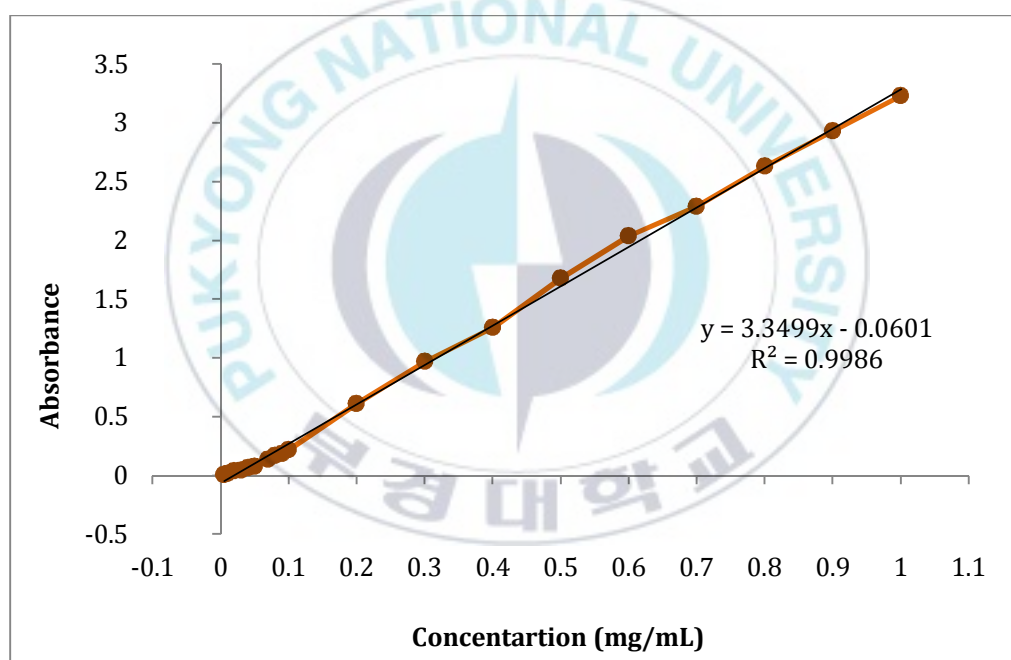


Figure 4.11. BR standard curve

The BR dilution series were oxidized after 24 hr exposure to air and became biliverdin (oxidized BR: green color). The standard curve and formula of BV were evaluated by measuring each dilution series absorbance at 660 nm (Figure 4.12.).

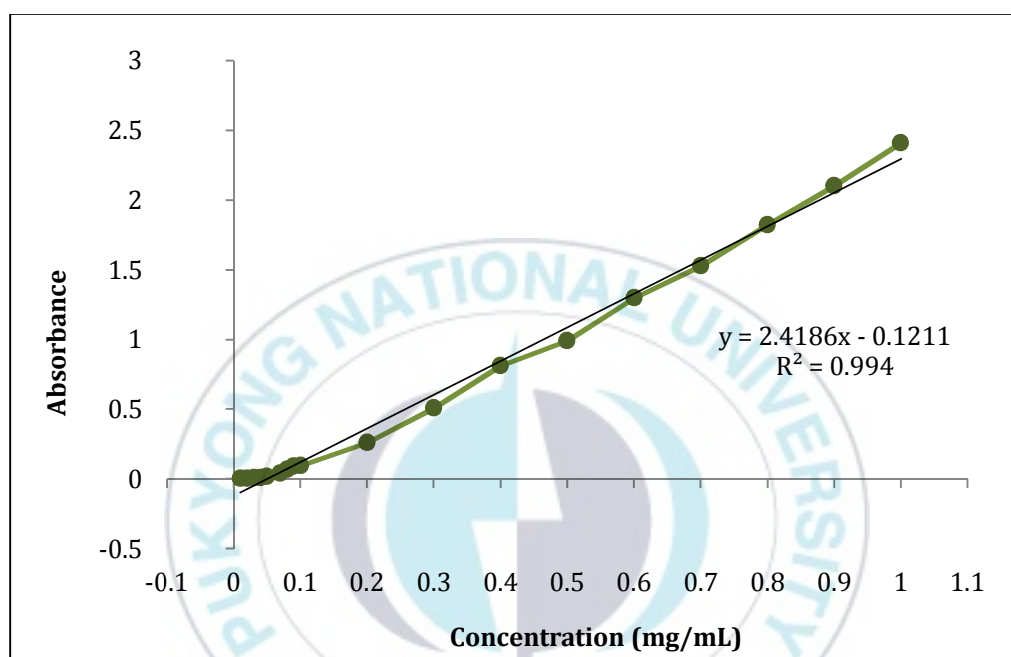


Figure 4.12. BV standard curve

#### 4.4. DRUG ENCAPSULATION

The BR was encapsulated in BSA-NPS according to the desolvation method and purified by centrifuge. UV-spectrophotometer confirmed the drug encapsulation by scanning the absorbance of free BR, naked BSA-NPS, and BSA-BR-NPS from 200 nm to 700 nm (Figure 4.13.) and compared to each other. The naked BSA-NPS and BSA-BR-NPs had an absorbance peak around 220 nm, which related to the BSA, and

confirmed the NPs character.

The BSA-BR-NPS and free BR have the same peak, around 440 nm, which refers to BR structure and its benzene groups and confirms the existence of BR inside BSA-BR-NPS, while the naked BSA-NPS do not have any absorbance at this wavelength.

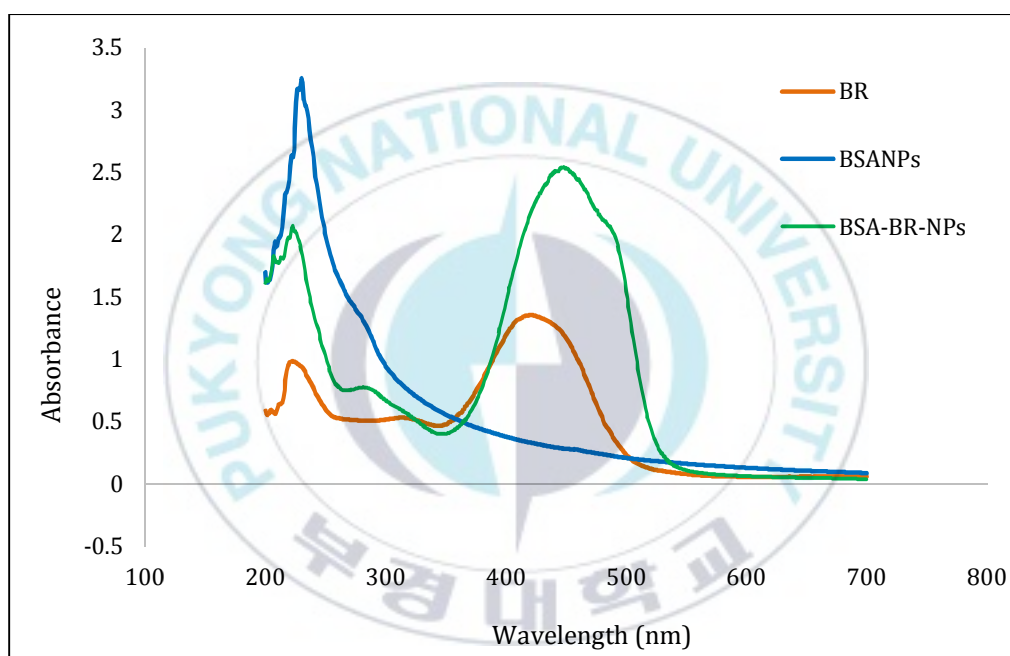


Figure 4.13. BSA-BR-NPs, drug encapsulation, a wave scan

The amount of encapsulated drugs was measured by UV-Spectrophotometry according to the standard BR calibration formula.

The free BR after nanoparticle preparation was measured, and the encapsulated drug

was calculated. The BSA-BR-NPS encapsulated 65.56% of the initial drug added to the mixture, which is around 6.555 mg (Table 4.4.).

Table 4.4. NPs characterization, E.E %

Formulation	Initial Drug (mg)	Free Drug (mg/mL)	Supernatant Volume (mL)	Encapsulated Drug (mg)	E.E %
BSA-BR-NPS	10	0.264	13	6.555	65.56

The BSA-BR-NPS were lyophilized after purification, the drug loading percent was calculated according to the total NPS weight and the encapsulated amount of the drug inside NPS (Table 4.5.). The D.L% for the BSA-BR-NPS was 10.8% after freeze-drying among 61 mg NPS.

Table 4.5. NPs characterization, D.L %

Formulation	Initial Drug (mg)	Encapsulated Drug (mg)	NP weight (mg)	D.L %
BSA-BR-NPS	10	6.555	61	10.8

#### 4.5. RELEASE ASSAY

In vitro release profiles of the BR was measure by mimicking two different conditions, normal (PBS, pH 7.4, 37 °C) and inflammation (PBS, pH 5.4, 42 °C, 0.1 M H<sub>2</sub>O<sub>2</sub>) conditions. After releasing from the NPS, the BR oxidized due to the oxygen in the air and the hydrogen peroxide in the system and became soluble BV. The amount of released drug was calculated according to the BV standard calibration formula. The final amount of released drug was measured by adding the drug released at each time point, 0.5, 1, 2, 3, 4, 5, 6, 10, 20, 24, and 48 hr.

The cumulative released amount of drugs from BSA-BR-NPS in normal conditions was around 15% of the total drug encapsulated (Figure 4.14.). Moreover, the cumulative released amount of drugs from BSA-BR-NPS in inflammation condition was around 66% of the total drug encapsulated (Figure 4.15.), which was higher than the released amount in normal condition due to the lower pH, higher temperature, and ROS situation (Figure 4.16.).

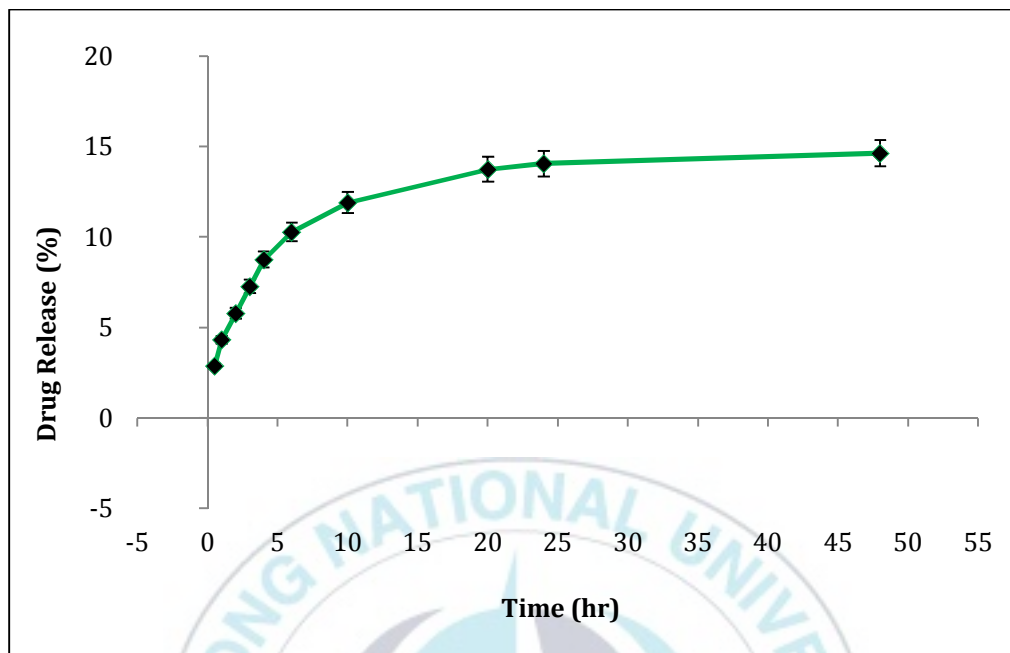


Figure 4.14. BR release profile from BSA-BR-NPs in normal condition

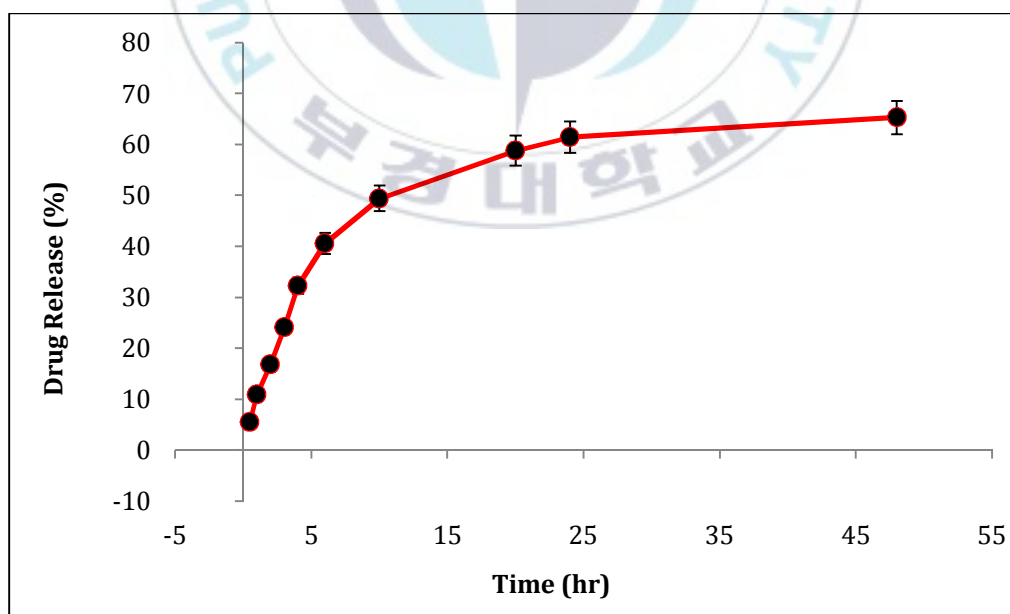


Figure 4.15. BR release profile from BSA-BR-NPs in inflammation condition

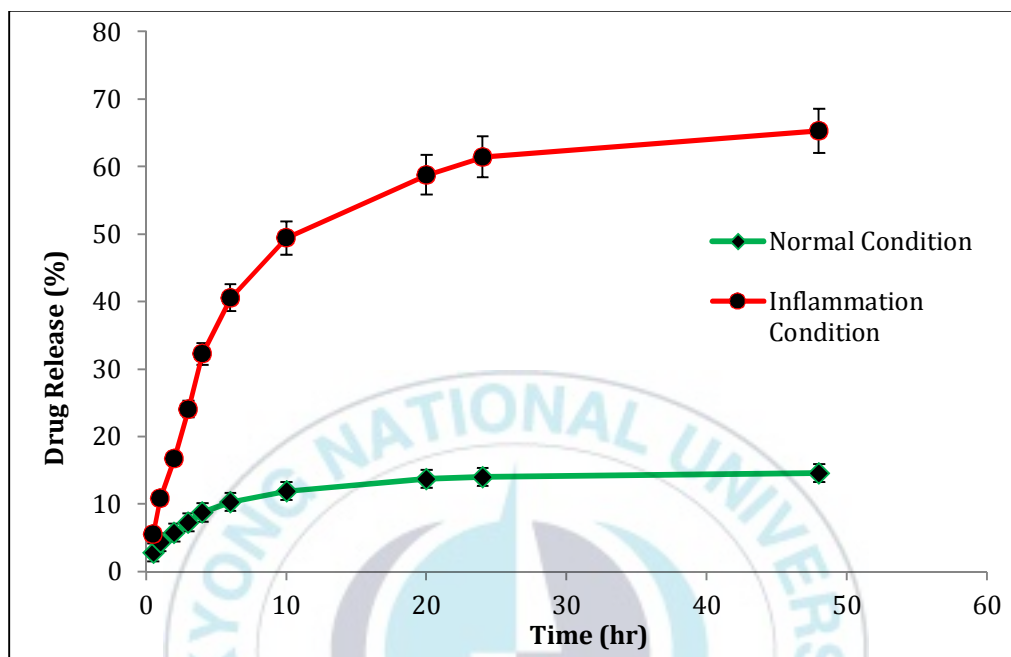


Figure 4.16. BR release profile from BSA-BR-NPs, comparison

## **4.6. FREE-RADICAL SCAVENGING**

### **4.6.1. DPPH FREE-RADICAL SCAVENGING ACTIVITY**

The anionic free-radical scavenging activity of the BSA-NPs and BSA-BR-NPS was measure using the DPPH method. The BSA-NPs and BSA-BR-NPs were mixed with the DPPH solution and incubated, and the scavenging rate was calculated using UV-Spectrophotometer.

The BSA-BR-NPs showed a dose-dependent manner in DPPH radical scavenging activity; the sample with 171.00  $\mu\text{M}$  concentration of BR showed the highest activity, around 90%, while the lower concentrations had lower scavenging activity to 30% for 21.37  $\mu\text{M}$  concentration.

BSA-NPS did not have any free-radical scavenging in different dosages in this assay. The particular reason for this circumstance is the natural feature of albumin that scavenges the cationic radicals, and it does not scavenge the anionic free radicals like DPPH (Figure 4.17.).

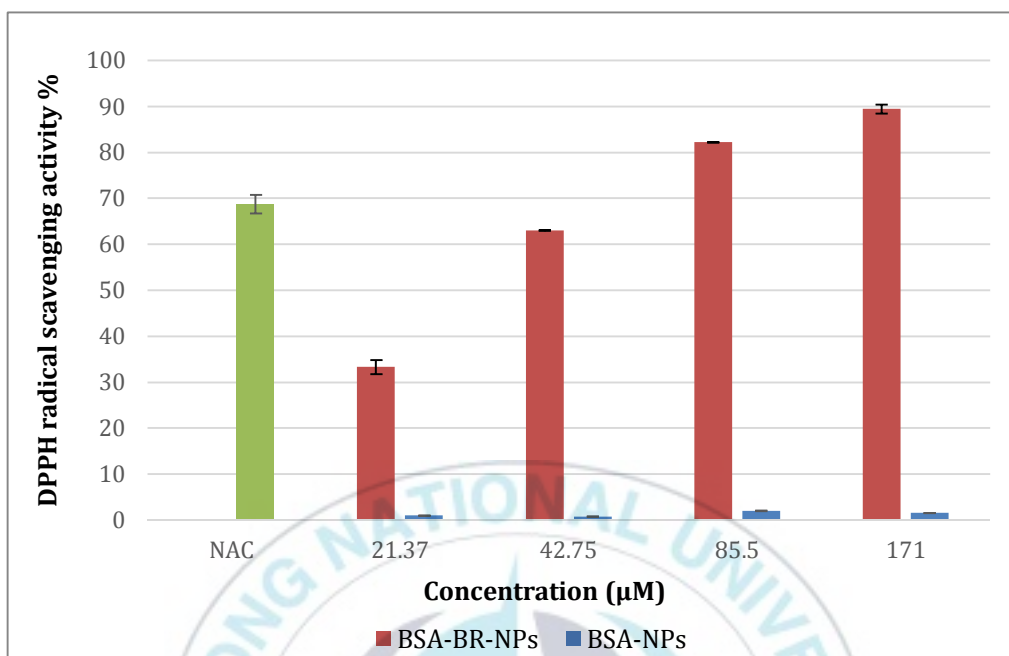


Figure 4.17. DPPH radical scavenging

#### 4.6.2. ABTS FREE-RADICAL SCAVENGING ACTIVITY

The cationic free-radical scavenging activity of the BSA-NPs and BSA-BR-NPs was evaluated by the ABTS method. ABTS solution was mixed with BSA-NPs and BSA-BR-NPs and incubated, and subsequently, the absorbance was recorded using UV-spectrophotometer.

The BSA-NPs illustrated a favorable cationic free-radical scavenging in comparison to anionic radicals scavenging. The scavenging activity of BSA-NPs increased from

35% for 21.37  $\mu\text{M}$  concentration of NPs to 60% for 85.50  $\mu\text{M}$ , and it remains stable at the higher dose.

The BSA-BR-NPs, showed high efficiency in cationic free-radical scavenging tests, according to its natural carrier and the payload. The effect of the encapsulated BR is evident in the scavenging activity of the same formulations in the exact dosages. The BSA-BR-NPs with 171.00  $\mu\text{M}$  concentration of BR scavenged almost all the free radicals, while the BSA-NPs scavenged around 60% of the ABTS. The ABTS free-radical scavenging activity of BSABR-NPs increased from 60% at the lowest dose of 21.37  $\mu\text{M}$  concentration to 99% at the highest concentration, 171.00  $\mu\text{M}$  (Figure 4.18.).

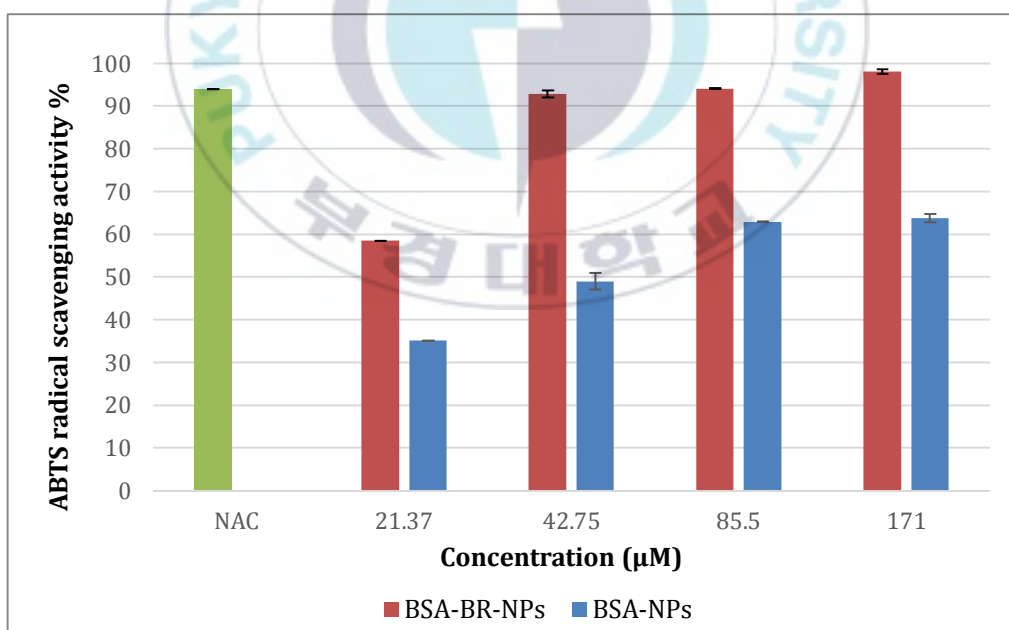


Figure 4.18. ABTS radical scavenging

## **4.7. CELL ASSAY**

The in-vitro cellular efficiency of the BSA-NPs, and BSA-BR-NPS and its toxicity on normal and cancer cells were investigated by MTT assay, using different normal and cancerous cell lines.

### **4.7.1. MTT ASSAY**

#### **4.7.1.1 NORMAL CELLS**

The toxicity of BSA-NPs, and BSA-BR-NPs on normal cells in the body, were measured by treating the CCD18-co (human normal colon fibroblast cells), BEAS-2B (human non-tumorigenic lung epithelial cells), and NHA (human normal astrocyte cells) cell lines with 0, 42.75, 85.50, 171.00, 256.51  $\mu\text{M}$  of samples w.r.t. BR concentration, for 24 h and 48 h. And then, the cell viability was calculated by spectrophotometry using SYNERGY HTX (Biotek) and compared with the control group.

The Naked-BSA-NPs did not show any toxicity on normal colon cells (CCD-18 co). The Free-BR group had toxicity on this cell line and at the dose of 85.50  $\mu\text{M}$  showed around 70% toxicity that remains the same in higher doses according to BR's poor water solubility, precipitated in the wells. The BSA-BR-NPs could successfully harvest the toxicity of BR on normal cells and showed a biocompatible profile. The toxicity of BR at the dose of 85.50  $\mu\text{M}$  decreased from 70% to 10% in encapsulated form (Figure 4.19.).

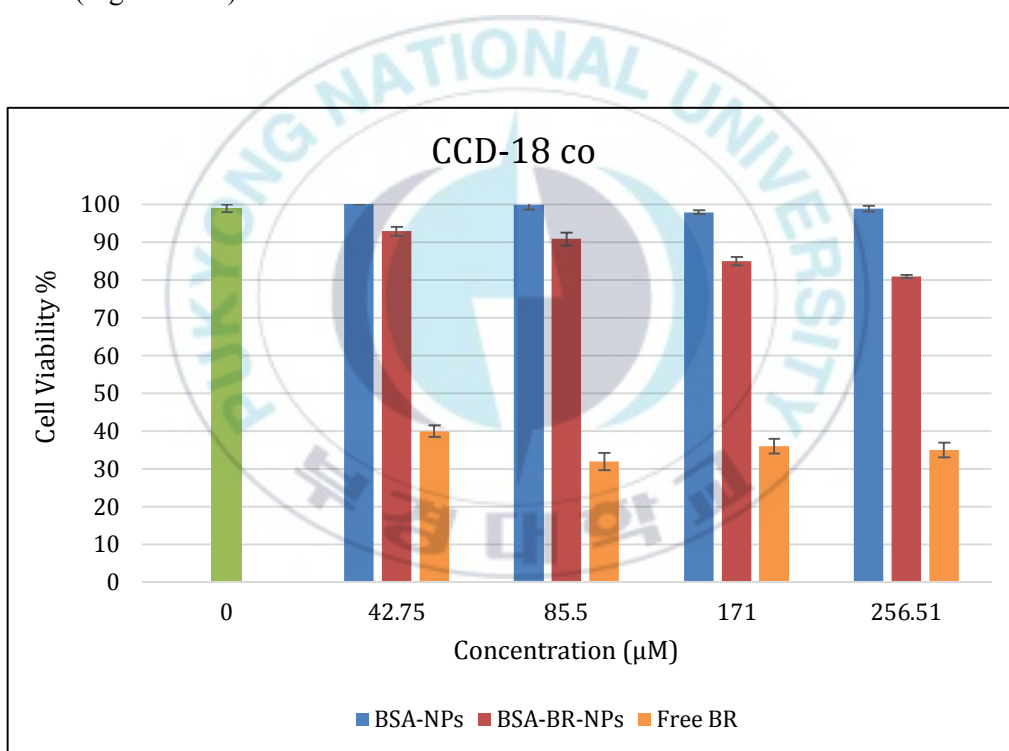


Figure 4.19. MTT-assay on CCD18-co cell line

The Free-BR had high toxicity on BEAS-2B (normal lung cells) cell line and showed more than 70% toxicity in different dosages. On the other hand, encapsulated BR, the BSA-BR-NPs had low toxicity on these cells, and at the highest dose, 256.51  $\mu\text{M}$ , it had around 13% toxicity which is too much lower in comparison to the Free-BR with the same concentration.

The Naked-BSA-NPs also did not have any toxicity on this cell line even at the highest doses (Figure 4.20.).

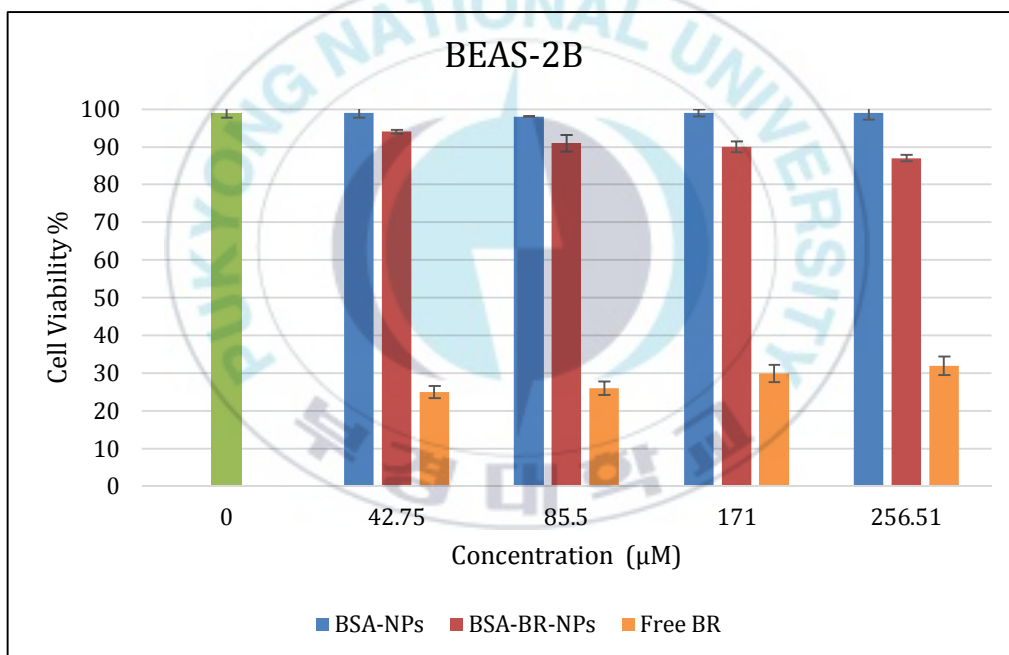


Figure 4.20. MTT-assay on BEAS-2B cell line

The third normal cell line investigated in this study is NHA (normal astrocyte cells) cell line. The BSA-NPs showed a non-toxic activity on this cell line and other normal cells, confirming its biocompatibility and safety to normal cells in the body.

The Free-BR had a toxic profile on this cell line, and its toxicity decreased depending on its dose due to the poor water insolubility, and it had around 50% toxicity at the highest dose, 256.51  $\mu\text{M}$ .

BSA-BR-NPS did not have significant toxicity on this cell line, at the same BR concentration, which means the drug did not release from the NPS in a normal situation and had only 12% toxicity on the highest dosage, it is 40% lower than free BR at the same concentration (Figure 4.21.)

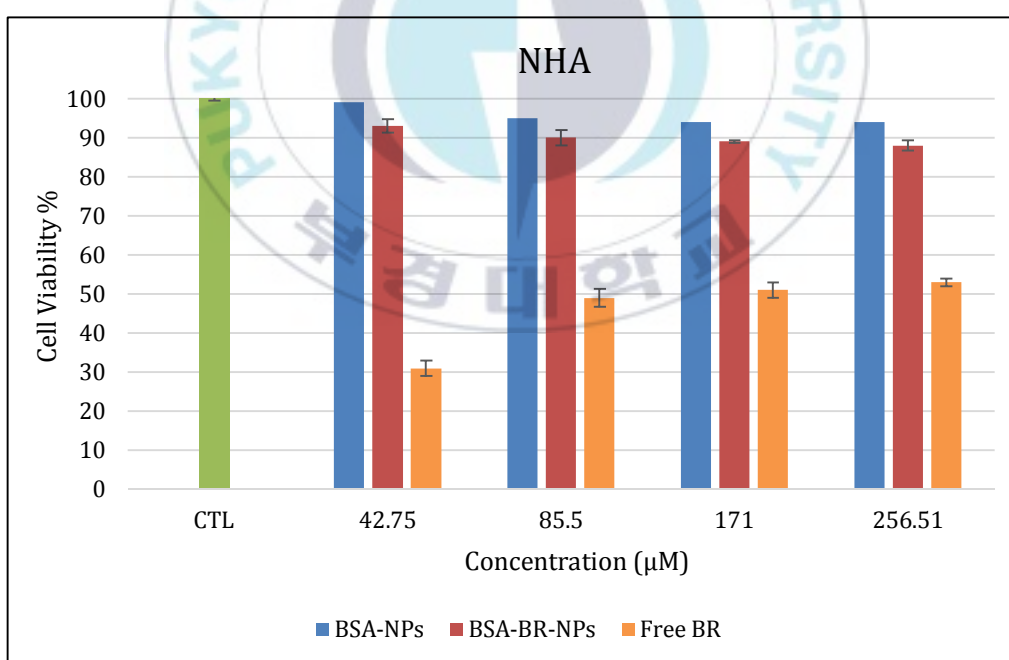
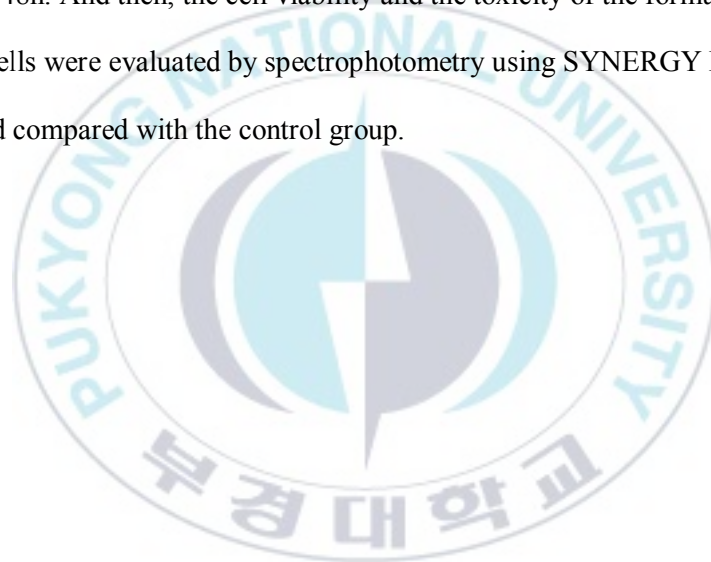


Figure 4.21. MTT-assay on NHA cell line

#### 4.7.1.2. CANCER CELLS

The efficiency of BSA-NPs and BSA-BR-NPs on cancer cells were investigated by treating the DLD-1 (colorectal adenocarcinoma cells), LN229 (human brain glioblastoma cells), SKOV-3 (ovarian cancer cells), CAOV-3 (primary ovarian cancer cells), SW480 (colon cancer cells), and HCT116 (colorectal adenocarcinoma cells) cell lines with 0, 42.75, 85.50, 171.00, 256.51  $\mu\text{M}$  of samples w.r.t. BR concentration, for 24h and 48h. And then, the cell viability and the toxicity of the formulations on cancerous cells were evaluated by spectrophotometry using SYNERGY HTX (Biotek) and compared with the control group.



On the DLD-1 (colorectal adenocarcinoma) cell line, the BSA-NPs had no toxicity compared to the control group.

The free-BR showed toxicity around 30% in different doses, while the encapsulated-BR in NPs, BSA-BR-NPs, had a higher efficiency and killed 40% of the cancer cells at 42.75  $\mu$ M concentration which is 30% higher than free-BR with the same concentration. In higher doses, it had the same efficiency as well (Figure 4.22.).

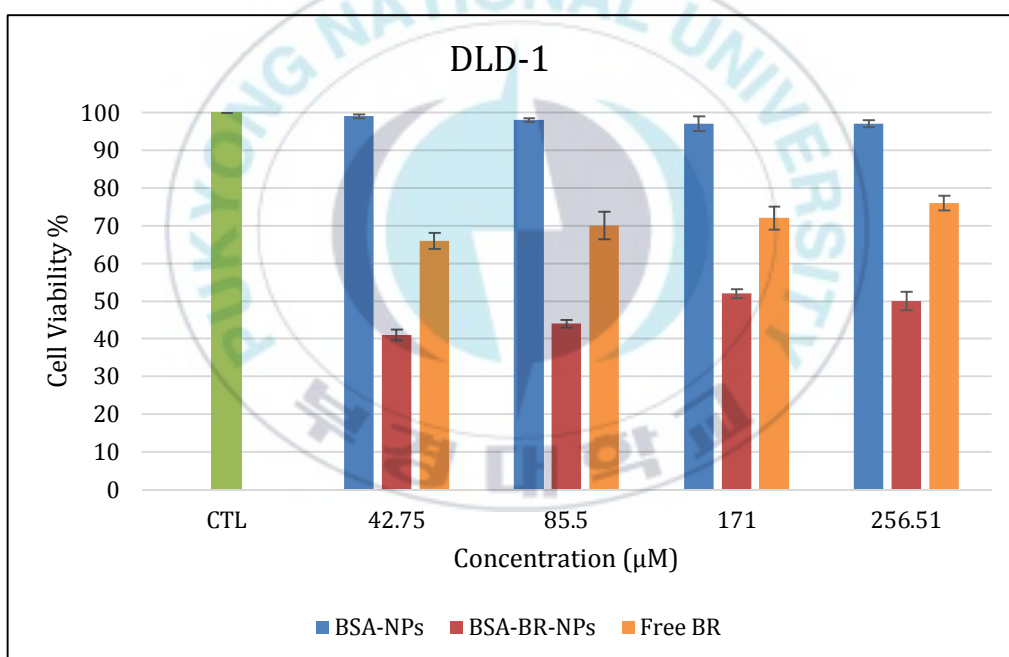


Figure 4.22. MTT-assay on DLD-1 cell line

On the LN-29 (human brain glioblastoma) cell line, the cells treated with naked BSA-NPs survived. However, 60% of the cells treated with 42.75  $\mu$ M BSA-BR-NPS w.r.t BR concentration were killed, and this amount increased to 95% of the cells at the highest concentration, 256.51  $\mu$ M, and showed a dose-dependent manner in this experiment.

Free-BR killed 30% of the cancerous cells at the highest concentration, which is 14 times lower than the same concentration in NPS format (Figure 4.23.).

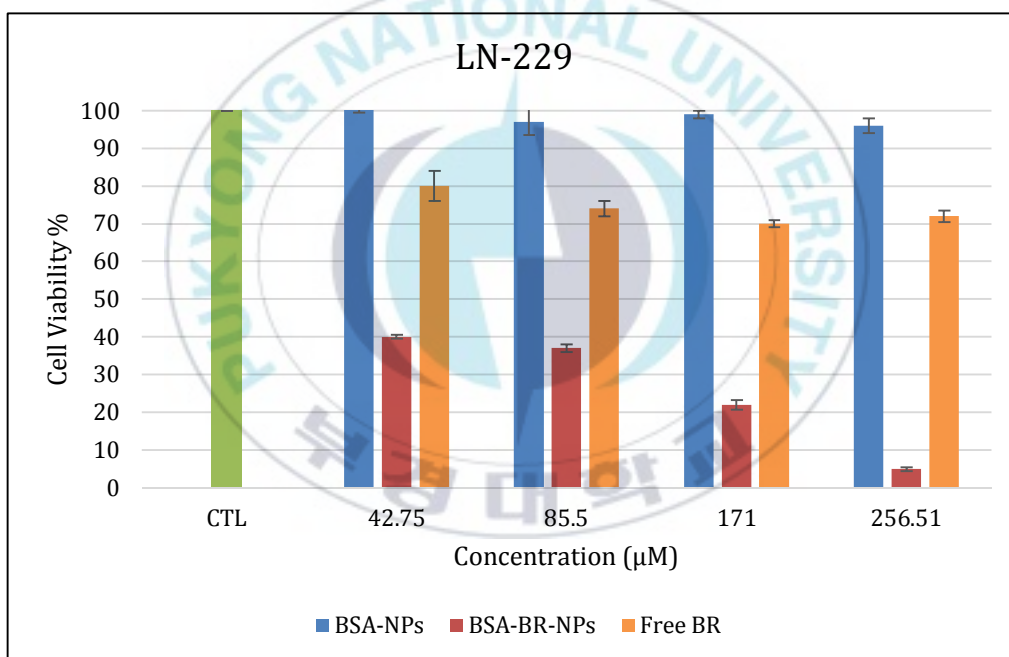


Figure 4.23. MTT-assay on LN229cell line

The SKOV-3 (ovarian cancer) cell line, were investigated and treated with three samples. The group treated with BSA-NPs did not show any toxicity, while the group treated with BSA-BR-NPs were killed in a dose-dependent profile. At the concentration of 42.5  $\mu\text{M}$ , 75% of the cancerous cells treated with BSA-BR-NPs were killed, and it increased to 90% of the cells at the concentration of 256.51  $\mu\text{M}$ . Free-BR showed 40% toxicity at the lowest dose and the highest dose, 256.51  $\mu\text{M}$  it increased only 10% (Figure 4.24.).

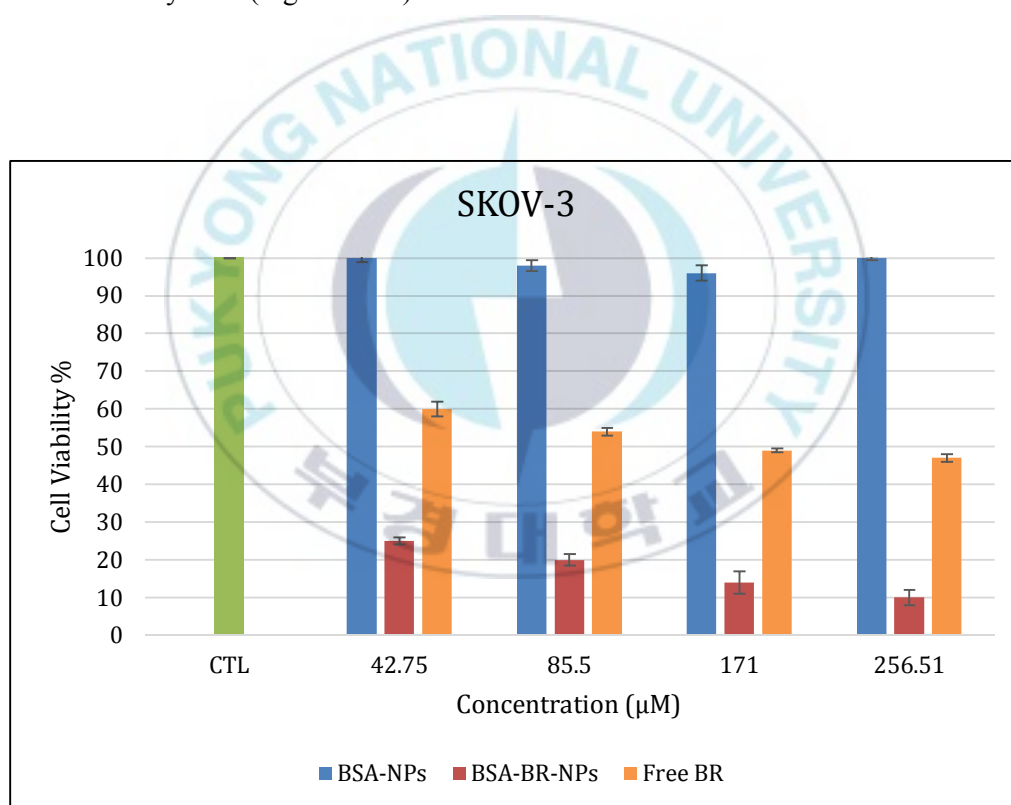


Figure 4.24. MTT-assay on SKOV-3 cell line

The BSA-NPs did not show toxicity on CAOV-3 (primary ovarian cancer) cell line. The BSA-BR-NPS had 40% toxicity at the lowest concentration, and it increased to 65% toxicity at the highest concentration, 256.51  $\mu$ M with a dose-dependent manner. The free-BR showed higher toxicity than BSA-BR-NPS on this cell line and had around 70% toxicity at all concentrations (Figure 4.25.).

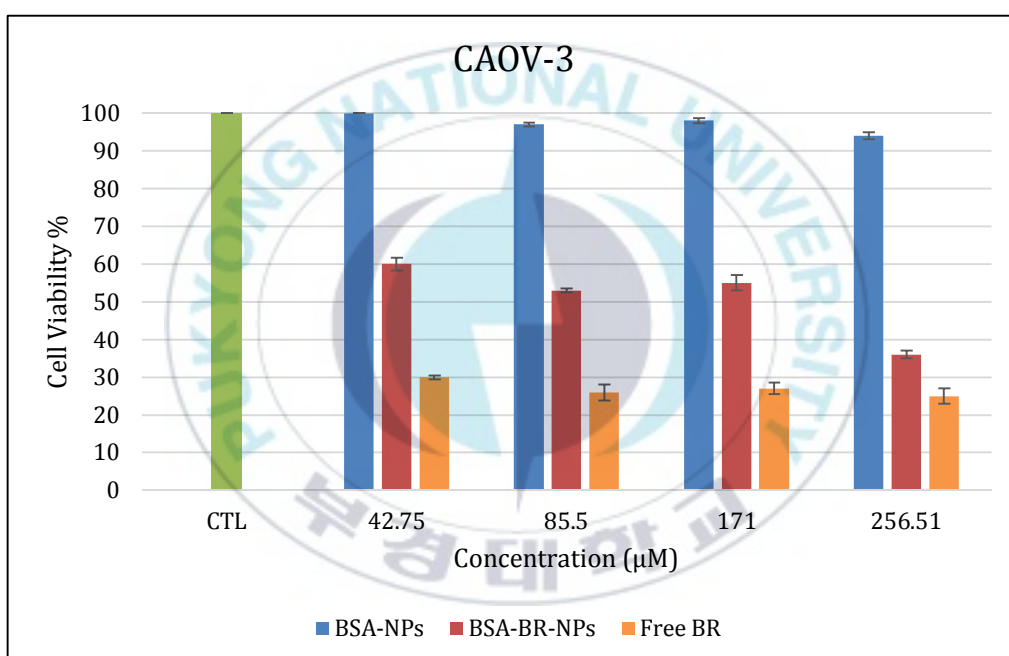


Figure 4.25. MTT-assay on CAOV-3 cell line

On SW-480 (colon cancer) cell line, the BSA-NPS had around 15% toxicity at the 256.51  $\mu\text{M}$  concentration.

The Free-BR had 10%, 60%, 40%, and 35% toxicity at the 42.75, 85.50, 171.00, 256.51  $\mu\text{M}$  concentrations, respectively. The reason for this fluctuation is probably the poor water solubility of BR at higher concentrations. This limitation addressed by encapsulating, and the toxicity of BSA-BR-NPS increased from 20% at the lowest concentration to 60% at the highest one.

At the 256.51  $\mu\text{M}$  concentration of the samples w.r.t BR, naked BSA-NPs had 15% toxicity, and free-BR had 35% toxicity, but the BSA-BR-NPS killed more than 60% of the cancerous cells (Figure 4.26.).

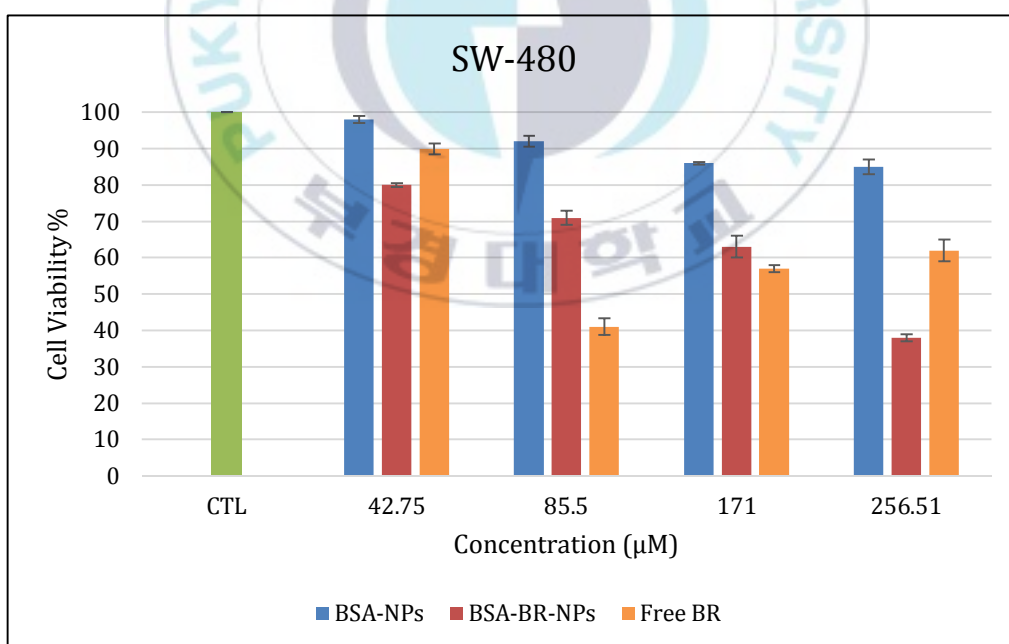


Figure 4.26. MTT-assay on SW480 cell line

On HCT-116 (colorectal adenocarcinoma) cell line, the BSA-NPs had more toxicity in comparison to other cell lines, and it killed 25% of the cancerous cells at the highest dose 256.51  $\mu\text{M}$ .

Free-BR showed the same toxicity at different concentrations and killed around 30% of the cells. While 40% of the cells treated with 42.75  $\mu\text{M}$  BSA-BR-NPS were killed, and this rate increased to around 60% of the cells at the highest dose.

At the dose of 256.51  $\mu\text{M}$ , the BSA-NPs, Free-BR, and BSA-BR-NPS had 25%, 30%, and 60% toxicity, illustrated the efficiency of nano-encapsulation and higher toxic activity of the drug in encapsulated form (Figure 4.27.).

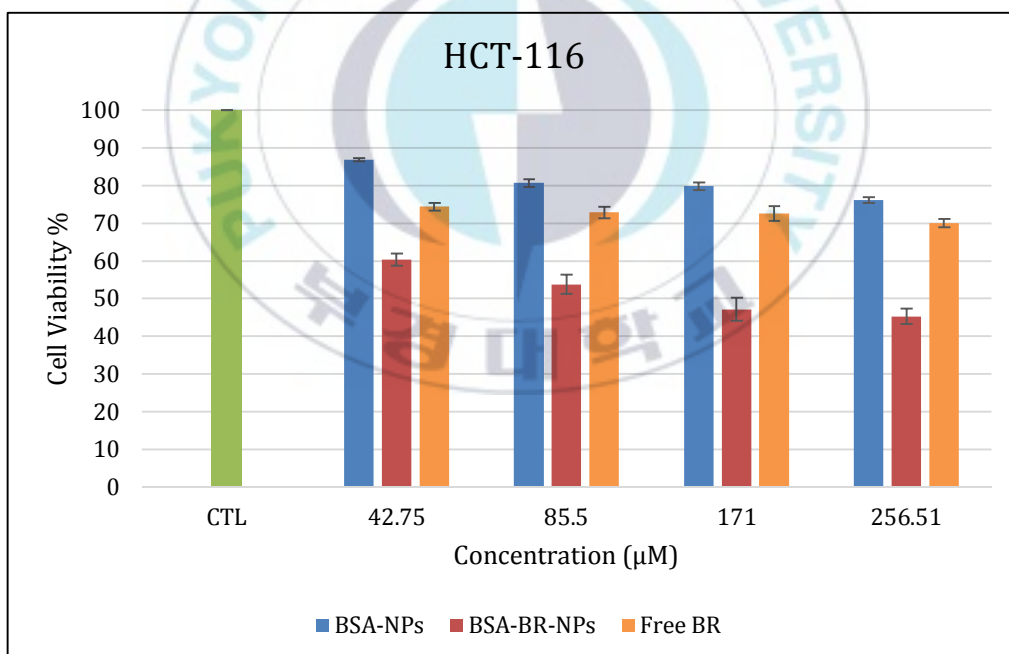


Figure 4.27. MTT-assay on HCT116 cell line

## CHAPTER 5: DISCUSSION AND CONCLUSION



In this study, we used Albumin to design and synthesize nanoparticles by a simple, cheap, and reproducible desolvation method. Albumin is a popular compound in drug delivery applications due to its biocompatibility, non-immunogenicity, long circulatory half-life, targeting ability and accumulating in malignant tissues, and binding capacity. Albumin can bind to different materials and act as the carrier or modify its functions through the bloodstream. Albumin has three homologous domains and a free thiol group, Cys-34, that works as a metal ions scavenger and is a primary element for albumin antioxidant activity.

Albumin nanoparticles have all the properties of single albumin nanoparticles while providing a high encapsulation efficiency and can encapsulate a drug inside or bind to another targeting or therapeutic component on the surface.

Bilirubin is a bile pigment, the final product of the heme catabolism pathway. BR is a toxic and water-insoluble compound. BR binds to SA as a carrier in the blood to travel through the tissues in the body. BR is a potent ROS scavenger and can quench different radical species and inhibit the oxidative stress condition.

After oxidation with ROS, BR change to biliverdin form. Biliverdin is a hydrophilic compound that can be reduced again to the BR.[50]

In an attempt to harness the therapeutic properties of bilirubin, investigators at Korea Institute of Advanced Science and Technology (KIAST) South Korea recently developed a water-soluble conjugate of bilirubin and polyethylene glycol (PEG), known as the bilirubin nanoparticle (BRNP). Since bilirubin is a lipophile and PEG is a hydrophile, the end product PEG-BR is an amphiphile, which self-assembles to

form a micelle-like structure or bilirubin nanoparticle around 140nm in size.[51, 52] BRNP treatment showed significant benefits in mouse models of different inflammatory conditions, such as asthma, colitis, pancreatic islet xenotransplantation, ischemia, and anticancer therapy.[53-55]

In another study, Wenzhou Medical University, China, investigated hyaluronic acid-coated bilirubin nanoparticles for treating acute kidney injury (AKI). This study coated e-polylysine-bilirubin (PLBR) nanoparticles with hyaluronic acid (HA-PLBR) and obtained particles around 228nm in size and spherical morphology. The in vitro and in vivo experiments show a high efficiency on the AKI rat model.[56]

Researchers from Shanghai Normal University, China, synthesized albumin-based nanoparticles which can encapsulate bilirubin and deliver it to the tumor environment. In this study, BSA-NPs were synthesized by galactosylated BSA using the sonochemical method, with a size around 300nm. The in vitro cellular assay and in vivo studies showed gal-BSA-NPs-BR have high efficiency in cancer treatment according to the bilirubin's ROS scavenging and antioxidant activity.[57]

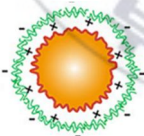
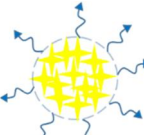
Different research groups attempt to employ BR in various applications according to antioxidant, anti-inflammation, and anticancer efficiency. In this trend, the limitations of BR, like its water insolubility, solved by polymeric conjugation and nanoparticle encapsulation. Although these studies were successful in vitro and in vivo studies, some issues should be considered. Polymeric conjugation such as PEGylation or hyaluronic acid conjugation requires multiple steps and high-risk processes, which were inappropriate for scaling up and moving to clinical studies and markets. Besides,

encapsulation and self-assembly of BR nanoparticles have been done by using highly toxic chemicals like chloroform, which has toxic potential in clinical studies and limitations in large-scale production.

This study used albumin nanoparticles, a popular drug carrier due to their biocompatibility, high encapsulation efficiency, and tumor microenvironment accumulation.

Abraxane® is the most famous albumin nanoparticle formulation, which contains paclitaxel as a payload and is produced by high-pressure homogenization technique. The albumin nanoparticles in this study were synthesized by a cheap and straightforward desolvation method, which has the capability to scale up without using highly toxic chemicals. In addition, the BR encapsulation was performed by the simple addition of desolvating agent, rather than using toxic chemicals, harsh conditions, or multiple conjugation steps (Table 4.6.).

Table 4.6. BR derivatives comparison

Formulation	Structure	Size	Fabrication Method	Application	Ref.
BSA-BR-NPS		164 nm	Desolvation	Anionic and Cationic ROS scavenging Cancer therapy	This study
PEG-BR-NPS		140 nm	Self-assembly (Polymer Conjugation)	ROS scavenging (H <sub>2</sub> O <sub>2</sub> ) Cancer Therapy Inflammation Therapy	[52]
HA-PLBR-NPS		228 nm	Self-assembly (Polymer Conjugation)	ROS scavenging Inflammation Therapy Acute Kidney Injury treatment	[56]
gal-BSA-BR-NPS		300 nm	Sonochemical	Liver Cancer Therapy	[57]

To sum up, everything that has been stated so far, the BSA-NPs made with desolvation method by adding a desolvating agent to the solvent phase. The BSA-NPs had a homogenous spherical shape under electron microscopy, size around 120 nm, and zeta potential around -29 mV. In comparison to polymeric conjugation like PEGylation and physio-chemical methods like sonication, this process is more accessible, cheaper, and has reproducibility and large-scale possibility.

The nanoparticles could successfully encapsulate around 66% of the BR inside with almost 11% loading efficiency. The size of the NPs increased to 164 nm after BR encapsulation, and their zeta potential became slightly positive to around +22 mV. The nanoparticles made with the sonochemical method had the size  $300 \pm 20$  nm that is two times bigger, while the EE% and D.L% are almost the same as our findings. The Hyaluronic acid-coated BRNPs had a bigger size, around 228 nm, measured after polymerization, self-assembly, and HA-Coating process.

The BSA-BR-NPS released 15% of the drug-loaded inside in the normal physiological condition (PBS, pH 7.4, 37 C), so this nanoparticle can protect the normal cells in the body from toxic BR payload. While in cancerous and oxidative stress conditions, the BSA-BR-NPS released almost 65% of the encapsulated drug to the released media after 48 h (PBS, pH 5.4, 42 C, H<sub>2</sub>O<sub>2</sub> 0.1 M) in a controlled manner. This controlled-released feature helps the BR release from the NPS to scavenge the ROS in the tumor environment and protect it from rapid clearance and any immune response.

The BR release rate from other BSA-BR-NPS made by the sonochemical method was

around 70% in inflammation simulated condition and 30% in normal condition after 80 h, which is higher than BSA-BR-NPS in normal condition and will cause more side effects in vivo models.

The BSA-NPS and BSA-BR-NPS showed an outstanding efficiency in ROS scavenging analysis, and the BSA-BR-NPS scavenged almost all the free radicals at the highest dose (171.00  $\mu\text{M}$ ) in two different experiments, DPPH (anionic radicals) and ABTS (cationic radicals). The BSA-NPs scavenged just cationic free radicals in ABTS analysis, which confirmed its radical scavenging and metal binding property. Based on this ROS scavenging activity of our formulation, we investigated in vitro cellular assay to measure its efficiency in cancer treatment and its antioxidant activity. The HA-coated BR-NPS showed 60% radical scavenging in the intracellular ROS scavenging test, and the PEG-BRNPs quenched 80% of the ROS at the 200  $\mu\text{M}$  concentration that is lower than BSA-BR-NPS investigated in this study.

The BSA-NPs and BSA-BR-NPs showed favorable biocompatibility and safety to different normal cell lines at different concentrations, while the free-BR had a toxic activity on normal cells, and encapsulating could overcome this issue and prevent its side effects on normal cell lines.

The BR toxicity mechanism is due to its inhibition in cell regulatory reactions inside the cell. BR is a lipophilic compound and enters the cells through the lipid bilayer membrane and inhibits enzymatic systems and protein phosphorylation inside the cell, which is the primary toxic mechanism on BR in cells, normal and cancerous.

The BSA-NPs showed low toxicity on some cancerous cells like colon cancer; the particular reason for this toxicity is the cationic ROS scavenging activity of albumin.

The free-BR showed high toxicity on different cancer cells, while this cancerous cell killing did not increase by increasing the concentration of the drug. This lower toxicity is due to the poor water solubility of BR that in higher concentrations precipitated in the wells. The other reason could be the BR's rapid oxidation that dramatically decreases its therapeutic and ROS scavenging activities.

The BSA-BR-NPS addressed the limitation of free-BR and showed a high ROS scavenging and high toxicity on various cancer cells. This mechanism includes inhibiting cell regulatory reactions inside the cell and removing ROS inside and outside the cells. For instance, BR scavenges the free radicals, which make the lipid chain peroxidation and damage the cell membrane.[42, 45] By scavenging these reactive species, the cancer environment becomes more stable, and the cancer proliferation will stop. Besides, the angiogenesis and metastasis potentials will decrease by this ROS scavenging activity.[46, 47]

The BSA-BR-NPs had at least 20% toxicity on cancer cells at the lowest dose, while this efficiency rises to 95% at the highest dose, 256.51  $\mu\text{M}$ , in a dose-dependent manner. The BSA-BR-NPs had high toxicity on Ovarian and Colon cancer; they also killed a significant amount of brain tumor cells, demonstrating its high therapeutic efficiency and ROS scavenging activity.

## 활성산소를 제거하는 빌리루빈 함유 알부민 나노입자 제조와 치료적 응용

Moosavizadeh Seyedmohammad

부경대학교 일반대학원 화학공학과

### 요약

빌리루빈 (BR)은 담즙 색소이며 혈장에서 풍부하게 발생하는 헴 이화 작용의 최종 산물이다. 빌리루빈은 다양한 활성산소종 (ROS)과 자유 라디칼을 제거 할 수 있는 내인성 항산화 제로서 세포와 조직을 산화적 손상으로부터 보호하는 역할을 한다. 실제로, 수많은 실험 연구에서 항산화, 항 염증 및 항암 활성화에 대한 빌리루빈의 잠재력이 입증되었다. 그러나 낮은 물 용해도, 정상 세포에 대한 독성, 빠른 제거 및 산소에 대한 높은 민감도는 빌리루빈의 임상 개발을 제한하는 요소로 지목되어 왔다. 이때문에 빌리루빈을 안정적으로 캡슐화하고 작용 부위에 정해진 용량을 전달할 수 있는 적절한 약물 운반체가 필요하다.

한편, 알부민은 혈중 농도가 가장 높은 단백질로서 적절한 크기와 FcRn 결합 특성으로 인해 순환 반감기가 3 주에 달하는 특성을 지닌다. 또한 알부민은 내재적으로 영양소, 대사 산물, 금속 및 약물과 결합하는 능력을 가지고 있어 약물 전달체로서 개발되기에 유리하다. 더욱이, 알부민은 능동적 또는 수동적 방식으로 종양 또는 염증 조직에 국부 전달된다고 알려져 있다. 이러한 특성에 기반하여 최근 개발된 혈청 알부민 나노입자, 즉 BSA-NP 는 내부에 약물을 캡슐화하거나 표면에 다양한 유형의 치료제 접합하여 질환부위로 전달하는 데 사용되어왔다.

이 연구에서 우리는 탈용매화(desolvation) 방법을 통해 소수성 빌리루빈을 캡슐화하는 알부민 나노입자(BSA-BR-NP)를 합성하고 특성화하는 방법을 탐구하였다. 또한 나노입자의 ROS 소거, 생체 적합성 및

암세포에 대한 독성을 측정하였다. 본 연구의 제법으로 합성된 BSA-BR-NP 는 약 70 %의 수율과 164 nm 크기로 빌리루빈을 캡슐화했으며, 구형을 띠었다. 빌리루빈 포획 효율 (EE)은 약 66 % 였고 약물 로딩 (DL)은 약 11 %였다. BSA-BR-NP 는 라디칼 소거 측정에서 자유 라디칼의 90 % 이상을 소거 하였다. 정상 세포에 대한 독성시험에서 BSA-BR-NP 는 낮은 독성으로 우수한 생체 적합성을 보여주었다. 반면에 BS-BR-NP 는 암세포에 대해 상당한 독성을 보여 향후 암세포 특이적 항암제로서의 개발 가능성을 높여주었다.



## CHAPTER 6: REFERENCES



- [1] D. J. Betteridge, "What is oxidative stress?," *Metabolism*, vol. 49, no. 2, pp. 3–8, Feb. 2000, doi: 10.1016/S0026-0495(00)80077-3.
- [2] M. Murata, "Inflammation and cancer," *Environ. Health Prev. Med.*, vol. 23, no. 1, pp. 1–8, 2018, doi: 10.1186/s12199-018-0740-1.
- [3] G. Pizzino *et al.*, "Oxidative Stress: Harms and Benefits for Human Health," *Oxid. Med. Cell. Longev.*, vol. 2017, pp. 1–13, 2017, doi: 10.1155/2017/8416763.
- [4] M. Valko, D. Leibfritz, J. Moncol, M. T. D. Cronin, M. Mazur, and J. Telser, "Free radicals and antioxidants in normal physiological functions and human disease," *Int. J. Biochem. Cell Biol.*, vol. 39, no. 1, pp. 44–84, Jan. 2007, doi: 10.1016/j.biocel.2006.07.001.
- [5] R. Kohen and A. Nyska, "Oxidation of Biological Systems: Oxidative Stress Phenomena, Antioxidants, Redox Reactions, and Methods for Their Quantification," *Toxicol. Pathol.*, vol. 30, no. 6, pp. 620–650, 2002, doi: 10.1080/0192623029016672.
- [6] S. Toyokuni, K. Okamoto, J. Yodoi, and H. Hiai, "Persistent oxidative stress in cancer," *FEBS Lett.*, vol. 358, no. 1, pp. 1–3, Jan. 1995, doi: 10.1016/0014-5793(94)01368-B.
- [7] S. V. Avery, "Molecular targets of oxidative stress," *Biochemical Journal*, vol. 434, no. 2. Biochem J, pp. 201–210, 01-Mar-2011, doi: 10.1042/BJ20101695.
- [8] A. Martínez, M. Portero-Otin, R. Pamplona, and I. Ferrer, "Protein targets of oxidative damage in human neurodegenerative diseases with abnormal protein

- aggregates," *Brain Pathology*, vol. 20, no. 2. Brain Pathol, pp. 281–297, Mar-2010, doi: 10.1111/j.1750-3639.2009.00326.x.
- [9] S. Toyokuni, "Reactive oxygen species-induced molecular damage and its application in pathology," *Pathology International*, vol. 49, no. 2. Pathol Int, pp. 91–102, 1999, doi: 10.1046/j.1440-1827.1999.00829.x.
- [10] M. H. Guajardo, A. M. Terrasa, and A. Catalá, "Lipid-protein modifications during ascorbate-Fe 2+ peroxidation of photoreceptor membranes: Protective effect of melatonin," *J. Pineal Res.*, vol. 41, no. 3, pp. 201–210, Oct. 2006, doi: 10.1111/j.1600-079X.2006.00352.x.
- [11] M. F. Beal, "Oxidatively modified proteins in aging and disease," *Free Radic. Biol. Med.*, vol. 32, no. 9, pp. 797–803, May 2002, doi: 10.1016/S0891-5849(02)00780-3.
- [12] M. Dizdaroglu, P. Jaruga, M. Birincioglu, and H. Rodriguez, "Free radical-induced damage to DNA: Mechanisms and measurement," *Free Radic. Biol. Med.*, vol. 32, no. 11, pp. 1102–1115, Jun. 2002, doi: 10.1016/S0891-5849(02)00826-2.
- [13] B. Balasubramanian, W. K. Pogozelski, and T. D. Tullius, "DNA strand breaking by the hydroxyl radical is governed by the accessible surface areas of the hydrogen atoms of the DNA backbone," *Proc. Natl. Acad. Sci. U. S. A.*, vol. 95, no. 17, pp. 9738–9743, Aug. 1998, doi: 10.1073/pnas.95.17.9738.
- [14] V. Brezova *et al.*, "Role of radicals and singlet oxygen in photoactivated DNA cleavage by the anticancer drug camptothecin: An electron paramagnetic

- resonance study," *J. Phys. Chem. B*, vol. 107, no. 10, pp. 2415–2425, Mar. 2003, doi: 10.1021/jp027743m.
- [15] H. Esterbauer, R. J. Schaur, and H. Zollner, "Chemistry and biochemistry of 4-hydroxynonenal, malonaldehyde and related aldehydes," *Free Radical Biology and Medicine*, vol. 11, no. 1. Free Radic Biol Med, pp. 81–128, 1991, doi: 10.1016/0891-5849(91)90192-6.
- [16] S. Nigam and T. Schewe, "Phospholipase A2s and lipid peroxidation," *Biochimica et Biophysica Acta - Molecular and Cell Biology of Lipids*, vol. 1488, no. 1–2. Biochim Biophys Acta, pp. 167–181, 31-Oct-2000, doi: 10.1016/S1388-1981(00)00119-0.
- [17] G. Fanali, A. Di Masi, V. Trezza, M. Marino, M. Fasano, and P. Ascenzi, "Human serum albumin: From bench to bedside," *Mol. Aspects Med.*, vol. 33, no. 3, pp. 209–290, 2012, doi: 10.1016/j.mam.2011.12.002.
- [18] B. Friedrichs, "Th. Peters. Jr.: All about Albumin. Biochemistry, Genetics, and Medical Applications. XX and 432 pages, numerous figures and tables. Academic Press, Inc., San Diego, California, 1996. Price: 85.00 US \$.," *Food / Nahrung*, vol. 41, no. 6, pp. 382–382, 1997, doi: 10.1002/food.19970410631.
- [19] J. Ghuman, P. A. Zunszain, I. Petitpas, A. A. Bhattacharya, M. Otagiri, and S. Curry, "Structural basis of the drug-binding specificity of human serum albumin," *J. Mol. Biol.*, vol. 353, no. 1, pp. 38–52, 2005, doi: 10.1016/j.jmb.2005.07.075.
- [20] G. Sudlow, D. J. Birkett, and D. N. Wade, "The characterization of two

- specific drug binding sites on human serum albumin," *Mol. Pharmacol.*, 1975.
- [21] M. Fasano *et al.*, "The extraordinary ligand binding properties of human serum albumin," *IUBMB Life*. 2005, doi: 10.1080/15216540500404093.
- [22] D. Sleep, J. Cameron, and L. R. Evans, "Albumin as a versatile platform for drug half-life extension," *Biochimica et Biophysica Acta - General Subjects*, vol. 1830, no. 12. Elsevier B.V., pp. 5526–5534, 01-Dec-2013, doi: 10.1016/j.bbagen.2013.04.023.
- [23] G. J. Quinlan, G. S. Martin, and T. W. Evans, "Albumin: Biochemical properties and therapeutic potential," *Hepatology*, vol. 41, no. 6, pp. 1211–1219, 2005, doi: 10.1002/hep.20720.
- [24] B. Halliwell and J. M. C. Gutteridge, "The antioxidants of human extracellular fluids," *Arch. Biochem. Biophys.*, 1990, doi: 10.1016/0003-9861(90)90510-6.
- [25] M. Anraku, V. T. G. Chuang, T. Maruyama, and M. Otagiri, "Redox properties of serum albumin," *Biochimica et Biophysica Acta - General Subjects*. 2013, doi: 10.1016/j.bbagen.2013.04.036.
- [26] M. Taverna, A. L. Marie, J. P. Mira, and B. Guidet, "Specific antioxidant properties of human serum albumin," *Ann. Intensive Care*, vol. 3, no. 1, pp. 1–7, 2013, doi: 10.1186/2110-5820-3-4.
- [27] D. Sleep, "Albumin and its application in drug delivery," *Expert Opin. Drug Deliv.*, vol. 12, no. 5, pp. 793–812, May 2015, doi: 10.1517/17425247.2015.993313.
- [28] A. Parodi, J. Miao, S. M. Soond, M. Rudzińska, and A. A. Zamyatnin,

- "Albumin nanovectors in cancer therapy and imaging," *Biomolecules*, vol. 9, no. 6, pp. 1–23, 2019, doi: 10.3390/biom9060218.
- [29] S. Hong, D. W. Choi, H. N. Kim, C. G. Park, W. Lee, and H. H. Park, "Protein-based nanoparticles as drug delivery systems," *Pharmaceutics*, vol. 12, no. 7, pp. 1–28, 2020, doi: 10.3390/pharmaceutics12070604.
- [30] P. Zhao, Y. Wang, A. Wu, Y. Rao, and Y. Huang, "Roles of Albumin-Binding Proteins in Cancer Progression and Biomimetic Targeted Drug Delivery," *ChemBioChem*, vol. 19, no. 17. Wiley-VCH Verlag, pp. 1796–1805, 04-Sep-2018, doi: 10.1002/cbic.201800201.
- [31] J. E. Schnitzer and P. Oh, "Antibodies to SPARC inhibit albumin binding to SPARC, gp60, and microvascular endothelium," *Am. J. Physiol. - Hear. Circ. Physiol.*, vol. 263, no. 6 32-6, 1992, doi: 10.1152/ajpheart.1992.263.6.h1872.
- [32] A. Loureiro, N. G. Azoia, A. C. Gomes, and A. Cavaco-Paulo, "Albumin-Based Nanodevices as Drug Carriers," *Curr. Pharm. Des.*, vol. 22, no. 10, pp. 1371–1390, 2016, doi: 10.2174/1381612822666160125114900.
- [33] Q. Yang, C. Zhou, Q. Zhao, Z. Chu, D.-P. Yang, and N. Jia, "Sonochemical assisted synthesis of dual functional BSA nanoparticle for the removal of excessive bilirubin and strong anti-tumor effects," *Mater. Sci. Eng. C*, vol. 100, no. October 2018, pp. 688–696, Jul. 2019, doi: 10.1016/j.msec.2019.03.042.
- [34] A. Parodi, J. Miao, S. Soond, M. Rudzińska, and A. Zamyatnin, "Albumin Nanovectors in Cancer Therapy and Imaging," *Biomolecules*, vol. 9, no. 6, p.

218, Jun. 2019, doi: 10.3390/biom9060218.

- [35] K. Langer, S. Balthasar, V. Vogel, N. Dinauer, H. Von Briesen, and D. Schubert, "Optimization of the preparation process for human serum albumin (HSA) nanoparticles," *Int. J. Pharm.*, vol. 257, no. 1–2, pp. 169–180, 2003, doi: 10.1016/S0378-5173(03)00134-0.
- [36] C. Weber, C. Coester, J. Kreuter, and K. Langer, "Desolvation process and surface characterisation of protein nanoparticles," *Int. J. Pharm.*, vol. 194, no. 1, pp. 91–102, 2000, doi: 10.1016/S0378-5173(99)00370-1.
- [37] A. Jahanban-Esfahlan, S. Dastmalchi, and S. Davaran, "A simple improved desolvation method for the rapid preparation of albumin nanoparticles," *Int. J. Biol. Macromol.*, vol. 91, pp. 703–709, 2016, doi: 10.1016/j.ijbiomac.2016.05.032.
- [38] X. Wang, J. R. Chowdhury, and N. R. Chowdhury, "Bilirubin metabolism: Applied physiology," *Curr. Paediatr.*, vol. 16, no. 1, pp. 70–74, 2006, doi: 10.1016/j.cupe.2005.10.002.
- [39] Q. Yao, R. Chen, V. Ganapathy, and L. Kou, "Therapeutic application and construction of bilirubin incorporated nanoparticles," *J. Control. Release*, vol. 328, no. April, pp. 407–424, 2020, doi: 10.1016/j.jconrel.2020.08.054.
- [40] R. Stocker, Y. Yamamoto, A. McDonagh, A. Glazer, and B. Ames, "Bilirubin is an antioxidant of possible physiological importance," *Science (80-. )*, vol. 235, no. 4792, pp. 1043–1046, Feb. 1987, doi: 10.1126/science.3029864.
- [41] V. L. Sundararaghavan, S. Binopal, D. E. Stec, P. Sindhwani, and T. D. Hinds,

- "Bilirubin, a new therapeutic for kidney transplant?," *Transplant. Rev.*, vol. 32, no. 4, pp. 234–240, 2018, doi: 10.1016/j.trre.2018.06.003.
- [42] A. C. Boon, C. L. Hawkins, J. S. Coombes, K. H. Wagner, and A. C. Bulmer, "Bilirubin scavenges chloramines and inhibits myeloperoxidase-induced protein/lipid oxidation in physiologically relevant hyperbilirubinemic serum," *Free Radic. Biol. Med.*, vol. 86, pp. 259–268, 2015, doi: 10.1016/j.freeradbiomed.2015.05.031.
- [43] R. Stocker, A. F. McDonagh, A. N. Glazer, and B. N. Ames, "Antioxidant activities of bile pigments: Biliverdin and bilirubin," *Methods Enzymol.*, vol. 186, no. C, pp. 301–309, 1990, doi: 10.1016/0076-6879(90)86123-D.
- [44] P. Novák, A. O. Jackson, G. J. Zhao, and K. Yin, "Bilirubin in metabolic syndrome and associated inflammatory diseases: New perspectives," *Life Sci.*, vol. 257, no. July, pp. 1–6, 2020, doi: 10.1016/j.lfs.2020.118032.
- [45] Z. Chen *et al.*, "Bilirubin Nanomedicines for the Treatment of Reactive Oxygen Species (ROS)-Mediated Diseases," *Molecular Pharmaceutics*, vol. 17, no. 7. American Chemical Society, pp. 2260–2274, 06-Jul-2020, doi: 10.1021/acs.molpharmaceut.0c00337.
- [46] T. W. R. Hansen, "Bilirubin Brain Toxicity," *J. Perinatol.*, vol. 21, no. S1, pp. S48–S51, Dec. 2001, doi: 10.1038/sj.jp.7210634.
- [47] T. W. R. Hansen, "Mechanisms of bilirubin toxicity: Clinical implications," *Clin. Perinatol.*, vol. 29, no. 4, pp. 765–778, 2002, doi: 10.1016/S0095-5108(02)00053-2.

- [48] F. Zahir, G. Rabbani, R. H. Khan, S. J. Rizvi, M. S. Jamal, and A. M. Abuzenadah, "The pharmacological features of bilirubin: The question of the century," *Cell. Mol. Biol. Lett.*, vol. 20, no. 3, pp. 418–447, 2015, doi: 10.1515/cmble-2015-0012.
- [49] Q. Yao, R. Chen, V. Ganapathy, and L. Kou, "Therapeutic application and construction of bilirubin incorporated nanoparticles," *J. Control. Release*, vol. 328, no. September, pp. 407–424, 2020, doi: 10.1016/j.jconrel.2020.08.054.
- [50] Z. Chen *et al.*, "Bilirubin Nanomedicines for the Treatment of Reactive Oxygen Species (ROS)-Mediated Diseases," *Mol. Pharm.*, vol. 17, no. 7, pp. 2260–2274, May 2020, doi: 10.1021/acs.molpharmaceut.0c00337.
- [51] Y. Lee, S. Lee, D. Y. Lee, B. Yu, W. Miao, and S. Jon, "Multistimuli-Responsive Bilirubin Nanoparticles for Anticancer Therapy," *Angew. Chemie - Int. Ed.*, vol. 55, no. 36, pp. 10676–10680, 2016, doi: 10.1002/anie.201604858.
- [52] Y. Lee, H. Kim, S. Kang, J. Lee, J. Park, and S. Jon, "Bilirubin Nanoparticles as a Nanomedicine for Anti-inflammation Therapy," *Angew. Chemie Int. Ed.*, vol. 55, no. 26, pp. 7460–7463, Jun. 2016, doi: 10.1002/anie.201602525.
- [53] Y. Lee, K. Sugihara, M. G. Gilliland, S. Jon, N. Kamada, and J. J. Moon, "Hyaluronic acid–bilirubin nanomedicine for targeted modulation of dysregulated intestinal barrier, microbiome and immune responses in colitis, SUP," *Nat. Mater.*, vol. 19, no. 1, pp. 118–126, Jan. 2020, doi: 10.1038/s41563-019-0462-9.

- [54] J. Y. Kim *et al.*, "Bilirubin nanoparticle preconditioning protects against hepatic ischemia-reperfusion injury," *Biomaterials*, vol. 133, pp. 1–10, 2017, doi: 10.1016/j.biomaterials.2017.04.011.
- [55] D. E. Kim, Y. Lee, M. G. Kim, S. Lee, S. Jon, and S. H. Lee, "Bilirubin nanoparticles ameliorate allergic lung inflammation in a mouse model of asthma," *Biomaterials*, vol. 140, pp. 37–44, 2017, doi: 10.1016/j.biomaterials.2017.06.014.
- [56] Z.-W. Huang *et al.*, "Hyaluronic acid coated bilirubin nanoparticles attenuate ischemia reperfusion-induced acute kidney injury," *J. Control. Release*, p. 142972, Apr. 2021, doi: 10.1016/j.jconrel.2021.04.033.
- [57] Q. Yang, C. Zhou, Q. Zhao, Z. Chu, D. P. Yang, and N. Jia, "Sonochemical assisted synthesis of dual functional BSA nanoparticle for the removal of excessive bilirubin and strong anti-tumor effects," *Mater. Sci. Eng. C*, 2019, doi: 10.1016/j.msec.2019.03.042.